HHS Public Access

Author manuscript

Biomaterials. Author manuscript; available in PMC 2023 January 01.

Published in final edited form as:

Biomaterials. 2022 January ; 280: 121254. doi:10.1016/j.biomaterials.2021.121254.

Nitric Oxide Releasing Nanomatrix Gel Treatment Inhibits Venous Intimal Hyperplasia and Improves Vascular Remodeling in a Rodent Arteriovenous Fistula

Maheshika Somarathna[1,*], **Patrick Tj Hwang**[2,*], **Reid C Millican**[3], **Grant C Alexander**[2], **Tatyana Isayeva-Waldrop**[1], **Jennifer A Sherwood**[3], **Brigitta C Brott**[4], **Isabelle Falzon**[5], **Hannah Northrup**[5], **Yan-Ting Shiu**[6], **Chris J Stubben**[7], **John Totenhagen**[8], **Ho-Wook Jun**[2,#], **Timmy Lee**[9,#]

[1]Department of Medicine and Division of Nephrology, University of Alabama at Birmingham, AL, 35294, USA.

[2]Department of Biomedical Engineering, University of Alabama at Birmingham, AL, 35294, USA; Endomimetics, LLC, Birmingham, AL, 35242, USA.

[3]Endomimetics, LLC, Birmingham, AL, 35242, USA.

[4]Endomimetics, LLC, Birmingham, AL, 35242, USA; Department of Medicine and Division of Cardiovascular Disease, University of Alabama at Birmingham, AL, 35233, USA.

[5]Division of Nephrology and Hypertension, Department of Internal Medicine, University of Utah, Salt Lake City, UT, 84132, USA.

[6]Division of Nephrology and Hypertension, Department of Internal Medicine, University of Utah, Salt Lake City, UT, 84132, USA; Veterans Affairs Medical Center, Salt Lake City, UT, 84148, USA.

Address for Correspondence: Timmy Lee, M.D., M.S.P.H., F.A.C.P., F.A.S.N., Professor of Medicine, Department of Medicine, Division of Nephrology, University of Alabama at Birmingham, 1720 2nd Ave South, Birmingham, AL 35294-0007, txlee@uab.edu, Phone: 205-975-9322, Fax: 205-975-6288. [#]Ho-Wook Jun and Timmy Lee are co-corresponding authors. txlee@uab.edu.

[*]Maheshika Somarathna and Patrick Hwang contributed equally to this work as co-first authors

CRediT authorship contribution statement

Maheshika Somarathna: Conceptualization, Methodology, Investigation, Validation, Formal Analysis, Writing – original draft. **Patrick Hwang:** Conceptualization, Investigation, Validation, Formal Analysis, Writing – original draft / review & editing, Visualization, Project Administration, Funding Acquisition. **Reid Millican:** Investigation, Resources, Validation, Writing – review & editing, Visualization. **Grant Alexander:** Investigation, Formal Analysis. **Tatyana Isayeva-Waldrop:** Investigation, Validation, Formal Analysis. **Jennifer Sherwood:** Investigation, Validation, Formal Analysis, Writing – review & editing. **Brigitta Brott:** Writing – review & editing. **Isabell Falzon:** Investigation, Software, Formal Analysis, Writing – review & editing. **Hannah Northrup:** Investigation, Software, Formal Analysis. **Yan-Ting Shiu:** Investigation, Software, Formal Analysis, Writing – review & editing, Funding Acquisition. **Chris Stubben:** Bioinformatic Analysis of Transcriptomics, Writing-review and editing. **John Totenhagen:** Investigation, Software, Formal Analysis. **Ho-Wook Jun:** Conceptualization, Methodology, Writing – review & editing, Supervision, Funding Acquisition. **Timmy Lee:** Conceptualization, Methodology, Writing – review & editing, Supervision, Funding Acquisition.

Declaration of interests

The authors declare the following financial interests/personal relationships which may be considered as potential competing interests: Timmy Lee is a consultant for Boston Scientific and Merck. Patrick Hwang, Jennifer Sherwood, Reid Millican, Brigitta Brott, and Ho-Wook Jun are employees of Endomimetics. The remaining authors have no competing interests.

[7]Bioinformatics Shared Resource, Huntsman Cancer Institute, University of Utah, Salt Lake City, UT, 84112, USA.

[8]Department of Radiology, University of Alabama at Birmingham, AL, 35294, USA.

[9]Department of Medicine and Division of Nephrology, University of Alabama at Birmingham, AL, 35294, USA; Veterans Affairs Medical Center, Birmingham, AL, 35233, USA.

Abstract

Vascular access is the lifeline for hemodialysis patients and the single most important component of the hemodialysis procedure. Arteriovenous fistula (AVF) is the preferred vascular access for hemodialysis patients, but nearly 60% of AVFs created fail to successfully mature due to early intimal hyperplasia development and poor outward remodeling. There are currently no therapies available to prevent AVF maturation failure. First, we showed the important regulatory role of nitric oxide (NO) on AVF development by demonstrating that intimal hyperplasia development was reduced in an overexpressed endothelial nitric oxide synthase (NOS3) mouse AVF model. This supported the rationale for the potential application of NO to the AVF. Thus, we developed a self-assembled NO releasing nanomatrix gel and applied it perivascularly at the arteriovenous anastomosis immediately following rat AVF creation to investigate its therapeutic effect on AVF development. We demonstrated that the NO releasing nanomatrix gel inhibited intimal hyperplasia formation (more than 70% reduction), as well as improved vascular outward remodeling (increased vein diameter) and hemodynamic adaptation (lower wall shear stress approaching the preoperative level and less vorticity). Therefore, direct application of the NO releasing nanomatrix gel to the AVF anastomosis immediately following AVF creation may enhance AVF development, thereby providing long-term and durable vascular access for hemodialysis.

Keywords

Arteriovenous fistula; nitric oxide; endothelial nitric oxide synthase; intimal hyperplasia; vascular remodeling; nitric oxide releasing nanomatrix gel

1. Introduction

There are more than 600,000 patients with end stage renal disease in the United States requiring dialysis therapy [1]. Vascular access dysfunction remains a significant cause of morbidity and mortality in patients utilizing hemodialysis, and the annual cost for treatment totals over one billion U.S. dollars [2]. The vascular access is the “lifeline” for the hemodialysis patient, and a functioning and durable vascular access permits consistent and reliable dialysis therapy. Arteriovenous fistulas (AVFs), created by a direct anastomosis between a native artery and vein, are the preferred type of vascular access because they have substantially low rates of thrombosis, infection, and healthcare-related expenditures, provided they successfully mature for dialysis [3]. However, AVF maturation failure remains a major cause of morbidity, mortality, and hospitalization among hemodialysis patients [4]. Although AVFs are the preferred option for dialysis access, up to 60% of AVFs created fail to mature adequately for successful dialysis use. AVF maturation failure is due to a combination of early aggressive venous intimal hyperplasia development and poor outward

remodeling following AVF creation. At present, there are no effective therapies to promote AVF maturation.

In this study, we demonstrated the importance of the "endothelial nitric oxide synthase (NOS) – nitric oxide (NO)" system in AVF remodeling and presented an innovative approach with the potential to enhance AVF maturation in the clinical setting (Fig. 1). The endothelium plays an important role in regulating AVF development. Endothelial-derived NO is a key vasodilator and signaling molecule in vascular remodeling [5–10], and it has also been shown to inhibit intimal hyperplasia in arterial injury models [11–14]. Here, we first showed the important regulatory role of NOS3 on venous intimal hyperplasia formation by using mouse AVF models with different levels of NOS3 expression. This study, where overexpression of NOS3 reduced initial hyperplasia development in AVFs, supported the hypothesis that increasing and sustaining local NO bioavailability -concurrent with AVF creation- may inhibit AVF maturation failure, thus providing the rationale for the potential application of NO to the AVF.

Next, we developed an innovative therapeutic NO delivery system, which is a self-assembled nanomatrix gel, in order to provide sustained release of NO directly at the venous anastomosis of the AVF, the primary site of AVF pathology. The NO releasing nanomatrix gel was composed of peptide amphiphiles (PAs) that consisted of hydrophilic NO releasing functional peptide sequences coupled to hydrophobic tails. The amphiphilicity of the PAs drives self-assembly of PAs into cylindrical micelle nanofibers, which form a nanomatrix gel with the addition of calcium ions [15, 16]. For NO delivery, amine group from lysine (K) interacts with NO and forms the NO complex, called diazeniumdiolate, on the PA-KKKKK [17, 18]. Dissociation of NO from the surface of the PA nanomatrix gel can occur by hydrolysis, which provides initial burst release of NO. Then, the NO diffuses through the multi-layered PA nanofibrous matrix, which enables the nanomatrix gel to provide sustained release of NO in comparison to other NO releasing materials [17]. Additionally, the formation of the nanomatrix gel via cross-linking without addition of organic solvents or initiators provides excellent biocompatibility. Using a syringe, the NO releasing nanomatrix gel can be directly applied locally to the AVF to maximize NO delivery and prevent systemic complications. To our knowledge, it is the first time for direct perivascular application of the NO releasing nanomatrix gel to promote AVF maturation. Thus, animals with healthy kidney functions were used, in order to test the safety and tolerance of this new technology. In the present study, *in vivo* analysis of the NO releasing nanomatrix gel application at the rat AVF anastomosis was performed. We demonstrated that the NO releasing nanomatrix gel was successfully applied at the venous anastomosis of the rat AVF, and reduced both venous intimal hyperplasia and a proinflammatory mediator (monocyte chemoattractant protein-1; MCP-1) and other markers of inflammation compared to the control nanomatrix gel (without NO) treated group by histological, biological analysis, and transcriptomics analysis. In addition, enhanced AVF outward remodeling by the NO releasing nanomatrix gel treatment was analyzed using magnetic resonance imaging (MRI)-based computational fluid dynamics (CFD) analysis. This study provides an alternative approach for addressing AVF maturation failure through local and sustained delivery of NO from nanomatrix gel directly applied to the AVF.

2. Materials and methods

2.1. Surgical creation of rodent AVF.

All studies and experiments were approved by the University of Alabama at Birmingham Institutional Animal Care and Use Committee (IACUC) and were performed in accordance with National Institutes of Health guidelines. For the investigation of the role of NOS3 in AVF, three strains of mice weighing 20–25 grams were used in these experiments. C57BL/6 mice ($NOS3^{+/+}$; wild type) and NOS3 knockout mice ($NOS3^{-/-}$) on C57BL/6 background were purchased from Jackson Laboratories. Transgenic mice overexpressing the human NOS3 gene (NOS3 OE) on C57BL/6 background were described in previous publications [19, 20]. The varying NOS3 expression levels in these three mouse strains (before AVF creation) were confirmed by Western Blot in our previous publication [21]. AVFs were created as described in detail in our previous study [22]. Briefly, an end (vein) to side (artery) fistula was surgically created between the jugular vein and carotid artery.

For NO releasing nanomatrix gel application, rat AVFs were created in 12–16 week old male Sprague Dawley strain (Taconic Biosciences, Hudson, NY). The rats were anesthetized in a continuous anesthetic induction chamber at a concentration of 3–4% using oxygen enriched air and placed on a heated surface to maintain body temperature at 37°C during the procedure. Midline incision of the surgical area was performed to expose the femoral vasculature. The femoral artery and vein were carefully dissected by using a surgical microscope. Vascular clamps were placed as distally and proximally as possible in the vein and artery to stop blood flow in the region of anastomosis creation followed by ligating the vein as distally as possible using a 7.0 silk suture. A longitudinal incision was made in the middle of the artery, and the vein was transected using a microsurgical scissor just proximally to the ligation. Lumens of both vessels were then rinsed with heparin solution (100 IU/ml) until the vessels were clear of blood. Using 10–0 microsurgical sutures (Arosurgical, polyamide monofilament), an end-to-side anastomosis was created using the femoral vein (end) and femoral artery (side). After unclamping of the femoral vessels, dilation of the arterialized vein and patency was confirmed visually. Then, the nanomatrix gel or the control gel (without nitric oxide) was directly applied on the anastomosis site followed by closing the skin with 6.0 suture.

2.2. Preparation of the self-assembled PAs.

Peptides consisting of a matrix metalloproteinase-2 (MMP-2) mediated cleavage site (GTAGLIGQ) with an endothelial cell-adhesive sequence YIGSR (for PA-YIGSR) or a nitric oxide (NO) donating residue KKKKK (for PA-KKKKK) were synthesized using standard Fmoc-chemistry on an Advanced Chemtech Apex 396 peptide synthesizer [17, 23, 24]. The synthesized peptide sequences were linked to a C_{16} palmityl chain by alkylation to create the peptide amphiphiles (PAs). The two PAs (PA-YIGSR, PA-KKKKK) were mixed in a 9:1 ratio to form PA-YK as previously described [17, 23, 24]. NO gas was reacted with the lysine residues in PA-YK (1 wt.%; weight/volume) after argon gas purge in a glass round bottom flask overnight to form PA-YK-NO.

2.3. Self-assembly of NO releasing nanomatrix gels.

The NO releasing nanomatrix gel was created by combination of PA-YK-NO (75 μL of 1 wt.%) and PA-S (75 μL of 2 wt.%; which consists only of the MMP-2 sensitive sequence and C_{16} alkyl chain to create a stable gel) with $CaCl_2$ (20μL of 0.1M) [16]. The molar ratio (M_r) among PAs and calcium ions (PA-YK-NO/PA-S/$CaCl_2$) to form the nanomatrix gel was 1:1:0.5, as previously described [16]. The control nanomatrix gel without NO was also created by combination of PA-YK, PA-S, and $CaCl_2$ (M_r = PA-YK:PA-S:$CaCl_2$=1:1:0.5).

2.4. Rheology characterization.

To determine the viscoelastic properties of the nanomatrix gels, an AR2000 rheometer (TA Instruments, UK) was used. Briefly, the gel was placed on a circular, flat-plate construct about 10 mm in size and subjected to oscillatory stress to determine the dynamic oscillatory shear. Pre-shear was applied to obtain equilibrium. The storage modulus (G') and loss modulus (G") were measured over a frequency range of 0.1 – 10 Hz at 37°C.

2.5. NO release kinetics from the NO releasing nanomatrix gel.

The nanomatrix gels were placed to insert-wells in a 24 well plate. The nanomatrix gel in the insert-well was incubated with 1 mL of phosphate buffered saline (PBS) under physiological conditions in an incubator at 37°C, 5% CO_2, and normal nitrogen and oxygen levels. The incubated PBS was collected, frozen (−80°C), and replaced by fresh PBS at 1, 5, 9, 13, 17, 21, 24, and 28 days. The collected samples were analyzed using a Griess assay reagent in the Total NO kit (Thermo Fisher Scientific). From the samples, the nitrite (NO_2-; primary degradation product of NO) and the reduced NO_2- from nitrate (NO_3-) were measured using a Griess assay.

2.6 Evaluation of NO gel on smooth muscle cell proliferation in vitro.

Human aortic smooth muscle cells (SMCs) (16,000 cells per each well; Lonza, Walkersville, MD) were seeded in the 24 well plate and cultured overnight with 1.5 ml of SMC growth medium (SmGM-2 BulletKit; Lonza) at normal cell culture conditions (37°C, 95% humidity, 5% CO_2). Then, varied concentrations of PA-YK-NO (0.2, 0.5, 1, and 3 wt.%) containing nanomatrix gels were loaded in the cell culture insert wells (3.0 μm pore size membrane, Corning, NC) and treated to the SMCs in the 24 well plate. The SMCs with the gels were cultured for 3 days under fetal bovine serum (FBS) deprived condition. After 3 days, the SMCs were stained by conducting a live/dead viability assay (Molecular Probes Inc., OR) and were quantified using microplate reader (Excitation/emission, live signal: 485 nm/528 nm and dead signal: 528 nm/617 nm).

2.7. Nanomatrix gel degradation test.

To test gel degradation treated to the rat AVF, an infrared (IR) fluorescence NO releasing nanomatrix gel was created. The IR dye 800CW (Licor, Lincoln, NE) was conjugated to the lysine residues on the PA-KKKKK (1 wt.%) *via* ester linkage. 2 μl of IR conjugated PA-KKKKK was then incorporated into the NO releasing gel during gel formation. After rat AVF creation, the IR fluorescence NO releasing gel was implanted at the anastomosis site. The rat was sutured back up and allowed to recover for 24 hours. For imaging, the rat was

sedated using isofluorane and placed in the LICOR Pearl Trilogy machine (Lincoln, NE). The fluorescence of the implanted gel on the surgical site was imaged at various time points to observe the degradation of the gel over a 2-month time period.

2.8. MRI acquisition and data extraction.

Rats were imaged with anatomical and angiography MRI techniques to determine the AVF flow velocity and lumen geometry as in our previous mouse study [22], with modifications for rats detailed in the Supporting Information. AVF flow velocities at the proximal fistula vein, proximal artery, and distal artery were extracted from the gradient echo velocity mapping sequence. Geometric reconstructions of the AVF lumen were created from the T2-weighted fast spin echo sequence, from which AVF lumen area was calculated and tetrahedral 3D meshes were created as we described [22].

2.9. CFD simulation and post-processing.

3D volumetric meshes were used as the lumen domains with rigid blood vessel walls in CFD simulations. Boundary conditions for the CFD simulation were prescribed as in our previous mouse study [21] with a modification for rats, described in the Supporting Information. Fluid-wall shear stress (FWSS) and vorticity were calculated from the results of CFD simulations [21, 22].

2.10. Tissue harvesting and sacrifice.

Anesthetized mice and rats were euthanized by intracardiac perfusion with PBS for protein studies and 10% formalin for histology studies 7 days after AVF creation. AVFs were dissected for tissue harvest. AVF vein sections were obtained from the AVF at the vein anastomosis up to 4–6 mm thickness from the anastomoses.

2.11. Morphometric analysis.

Morphometric analysis from Masson’s trichrome staining (mouse model) and Russell-Movat pentachrome staining (rat model) was performed on each AVF to determine the average intimal/media area ratio as previously described [25, 26]. 10–12 slides of 5 μm sections were obtained by selecting the first of every 10 sections beginning at the vein anastomosis of the AVF. Digital photographs of each section were taken and processed using Adobe Photoshop Creative Suite 6. Cellsense Dimension Software (Olympus Life Science) was used for the morphometric analysis and was performed in photographs of stained tissue sections at the final magnification of 4X or 10X. Intimal area (Blue) and the medial area (Red) were outlined, and tissue areas were measured and recorded in square micrometers. The ratio of intimal area (Ia) to medial area (Ma) was calculated (Ia/Ma). For each animal, mean values for the intimal to medial area ratio were reported. In the mouse model, morphometry was also performed with Verhoeff-Van Gieson to compare morphometric analysis with Masson’s trichrome staining (Supporting Materials and Methods and Supplementary Fig.S2)

2.12. Western blotting analysis.

The AVF and control tissues were lysed using the cold radioimmunoprecipitation assay (RIPA) lysis buffer (Millipore, Billerica, MA) containing protease and phosphatase

inhibitors (Thermo Scientific, Waltham, MA). Equal amounts of protein (20 μg) were separated on 4–15% polyacrylamide gel (Bio-Rad, Hercules, CA) and then transferred from the gel to the nitrocellulose membrane (Thermo Scientific, Waltham, MA). The membranes were incubated with blocking solution (5% BSA) containing (1) MCP-1 (Cell Signaling, Beverly, MA #9572) and (2) interleukin-1 beta (IL1-β) (Abcam, Cambridge, MA, #Ab64179) antibodies. Equal loading of protein was confirmed by measuring total protein or GAPDH expression. Secondary antibodies were goat anti-mouse, goat anti-rabbit or chicken anti-goat antibodies, respectively, conjugated to horseradish peroxidase (HRP). Detection of the protein bands was performed using standard enhanced chemiluminescent (ECL) substrate (Thermo Scientific, Waltham, MA). Densitometric analysis was performed to quantitatively assess total protein expression from the Western blotting using Image J. The Image J quantitated intensity of bands was normalized to GAPDH.

2.13. AVF tissue cGMP analysis.

Snap-frozen samples at the time of vessel harvest were analyzed for cyclic guanosine monophosphate (cGMP; vasodilation mediator) using a commercial enzyme-linked immunosorbent assay (ELISA) kit (GenScript, Piscataway, NJ). cGMP levels were expressed as pmol/mg protein.

2.14. Immunohistochemical analysis.

Paraffin-embedded AVF venous sections from NO gel and control gel treated rats were evaluated to identify the cellular phenotypes contributing to the intimal hyperplasia formation. α-SMA (M0851, DACO Agilent, Santa Clara, CA), Vimentin (M0725, DACO Agilent, Santa Clara, CA) and Desmin (M0760, DACO Agilent, Santa Clara, CA) primary antibodies were used to verify the presence of cells with smooth muscle origin and the presence of myofibroblasts. In addition, CD68 (NB600–985, Novus Biologicals, Centennial, CO) primary antibodies were used to verify the presence of inflammatory cells.

2.15 Transcriptomics analysis

RNA extraction and sequencing—Outflow AVF vein samples were harvested from nitric oxide nanomatrix gel and control gel treated rats at postoperative day 7 and flash frozen with liquid nitrogen and stored at −80 degrees. RNA isolation and sequencing were performed by Discovery Life Sciences (Huntsville, AL). Total RNA was isolated using standard Discovery Life Sciences protocols. All samples underwent RNA quality control assessment using a Fragment Analyzer (Agilent) and had RNA Integrity Number (RIN) >9.0. All RNA samples that pass quality control underwent library preparation using the TruSeq™ Stranded Total RNA With Ribo-Zero™ Plus rRNA Depletion protocol (Illumina, San Diego CA). Quality control for library concentration estimation was performed using Picogreen assay (Invitrogen) and fragment size estimation was performed using the Caliper DNA-HS chip. Kapa qPCR quantification was performed to estimate the nanomolar concentration of the final libraries. RNA libraries were sequenced at 150 base pair read length to attain 50M paired-end reads (100M total reads) on a NovaSeq 6000 instrument (Illumina, San Diego, CA).

RNA sequencing bioinformatic analysis—The rat genome and gene feature files were downloaded from Ensembl release 104 (Rnor_6.0 assembly) and the reference database was created using STAR version 2.7.9a with splice junctions optimized for 100 base pair reads [27]. Optical duplicates were removed from the paired end FASTQ files using clumpify v38.34 and reads were trimmed of adapters using cutadapt 1.16 [28]. The trimmed reads were aligned to the reference database using STAR in two pass mode to output a BAM file sorted by coordinates. Mapped reads were assigned to annotated genes using featureCounts version 1.6.3 [29]. The output files from cutadapt, FastQC, FastQ Screen, Picard CollectRnaSeqMetrics, STAR and featureCounts were summarized using MultiQC to check for any sample outliers [30]. Differentially expressed genes were identified using a 5% false discovery rate with DESeq2 version 1.30.1 [31]. The differentially expressed genes were further analyzed in Ingenuity Pathway Analysis (IPA) to find enriched pathways and upstream regulators [32].

2.16. Statistical analysis.

Group comparisons for the mouse and rat AVF were performed by paired t-test (if data followed a normal distribution) or Wilcoxon signed-rank test (if data did not follow a normal distribution), with significance set at *$p<0.05$ and **$p<0.01$. Statistical comparisons of CFD-derived results (velocity, FWSS, and vorticity) were performed in GraphPad Prism 8 (GraphPad Software, Inc., La Jolla, CA) by one-way ANOVA with Tukey post-tests for individual comparisons, with significance set at *$p<0.05$.

3. Results

3.1. NOS3

Overexpression mice have reduced AVF intimal hyperplasia.—We investigated the role of NOS3 on AVF maturation by utilizing three mouse strains: NOS3−/− (knockout), NOS3+/+ (wild type), and NOS3 OE (overexpression). AVFs were created using end-to-side anastomosis of the internal jugular vein (end) to carotid artery (side) (Fig. 2a); the venous segment of the AVF anastomosis was harvested at 7 days to quantitate intimal hyperplasia formation by histology analysis, and to measure tissue cGMP levels using an ELISA. The histology at the 7-day time point demonstrated a marked reduction of intimal hyperplasia formation in NOS3 OE mice when compared to both NOS3−/− and NOS3+/+ mice. Furthermore, there was significant intimal hyperplasia formation in NOS3−/− mice when compared to NOS3+/+ mice, suggesting a deficiency in NOS3 expression may contribute to AVF maturation failure by promoting intimal hyperplasia formation (Fig. 2b–e). In addition, the degree of stenosis at the venous AVF demonstrated the same trends with the intimal hyperplasia development at the 7-day time point (Supplementary Fig. S1). NOS3 OE and NOS3+/+ mice showed a significant reduction of stenosis, resulting in increased open lumen percentage, at the venous AVF compared to NOS3−/− mice. Thus, NOS3 upregulation could play a beneficial role in AVF maturation by reducing intimal hyperplasia and stenosis following AVF creation.

In addition, cGMP (vasodilation mediator) expression in the venous portion of the AVF was measured in each mouse group. NO synthase-derived NO diffuses into the

surrounding layers of vascular smooth muscle cells to mediate vasodilation. NO produces vessel relaxation by activation of soluble guanylyl cyclase, which subsequently elevates intracellular cGMP levels in vascular smooth muscle cells [33, 34]. We found that cGMP levels at the venous anastomosis were significantly increased in NOS3+/+ and NOS3 OE mice compared to NOS3−/− mice (Fig. 2f).

Taken together, using a genetic approach, we found that the NOS3-NO-cGMP pathway is positively associated with reduced AVF venous intimal hyperplasia, and that upregulated NOS3 expression can promote desired AVF remodeling.

3.2. In vitro characterization of NO gel.

For the application of NO therapy on AVF maturation, the NO releasing nanomatrix gel was developed by co-assembly of PAs, consisting of PA-YK-NO (1 wt.%) and PA-S (2 wt.%) (Fig. 3a). PA-YK-NO contains enzyme-mediated degradable sites for nanomatrix remodeling, laminin-derived endothelial cell adhesive ligands, and poly-lysine NO donors in optimized ratios for a vessel healing strategy [17, 35]. PA-S has only enzyme-mediated degradable sites and higher mechanical stability compared to other PAs [16]. Thus, the combination of PA-S with functionalized PAs enables modulation of the viscoelastic properties and creation of a robust platform for *in vitro* and *in vivo* applications [16].

The viscoelastic properties of the NO releasing nanomatrix gel and the control gel without NO were analyzed using an AR Rheometer. The storage modulus (G') and loss modulus (G") of the gels were evaluated at variable frequencies at 37°C (Fig. 3b). The storage modulus (G') indicates elastic behavior and measures the stored deformation energy; both gels had a storage modulus (G') higher than 4,000 Pa at various frequencies up to 10 Hz. The loss modulus (G") is a measure of the energy dissipated as heat and friction when subjected to deformation. A ratio of storage modulus to loss modulus (G'/G") of both gels was also calculated, and the G'/G" values of both gels were higher than 3 at various frequencies as shown in the table. In general, a stable gel can be assumed if G'≥10 Pa for practical gel application and G'/G"≥1 is commonly used to indicate gel formation [16, 36]. Thus, the rheology data indicated that both the NO releasing nanomatrix gel and control gel have sufficiently robust viscoelastic properties for *in vivo* application.

In addition, the *in vitro* NO release profile from the nanomatrix gel was evaluated using the total NO assay kit (Thermo Fisher), which indirectly measures the accumulation of released NO from the nanomatrix gel, for a month. NO release was characterized as having an initial burst release in the first 24 hours (about 17% of the NO), followed by sustained release over a period of 28 days, with 72% of NO released (Fig. 3c). The burst release from dissociated NO on the surface of the nanomatrix gel was easily accessible to the AVF to promote immediate vasodilation. Then, sustained delivery was achieved as the NO within the nanomatrix gel slowly diffused through the multi-layered PA nanofibrous matrix, as well as by enzyme mediated nanomatrix degradation [17]. Prolonged NO release is critical to arrest intimal hyperplasia, maintain proper vasodilation, and enhance endothelialization during the recovery period after AVF creation, which may take a few weeks [37–39]. This NO release profile is consistent with our prior work on the degradation and release kinetics of the PA nanomatrix [17, 23].

We also evaluated the effects of NO releasing nanomatrix gel on human aortic smooth muscle cell (SMC) proliferation *in vitro*. For this experiment, we used varying concentrations of PA-YK-NO (0.2, 0.5, 1, and 3 wt.%) to create nanomatrix gels containing different NO concentrations (Fig. 3d,e). The concentration of NO releasing nanomatrix gel that inhibited SMC proliferation was used as a basis for gel application in the *in vivo* AVF model for the reduction of intimal hyperplasia. The prepared gels were treated to SMCs using insert wells and evaluated utilizing live/dead assays 3 days after gel treatment. In the live cell assay, the 0.2 wt.% PA-YK-NO containing gel treated group did not show a significant difference in live fluorescence signal compared to the untreated group. However, the 0.5 wt.% PA-YK-NO containing gel treated group showed a significant reduction in fluorescence when compared to the untreated group. Both 1 wt.% and 3 wt.% PA-YK-NO containing gel treated groups showed an additional reduction of fluorescence, but there was no significant difference between the two groups. In the dead cell assay, there was no significant difference in dead fluorescence signal among all groups. These results indicated that NO releasing nanomatrix gel reduced SMC proliferation at PA-YK-NO (>0.5 wt.%) concentrations but did not affect cell viability. Since 1 wt.% PA-YK-NO containing gel showed the highest reduction in SMC proliferation (3 wt.% did not significantly reduce further), this concentration of gel was used for the *in vivo* studies.

3.3. Degradation of NO gel applied to the AVF in rats.

Maintaining nanomatrix gel stability after application to the AVF is critical for sustained NO delivery and therapy. To evaluate gel degradation surrounding the AVF, we applied fluorescent NO releasing nanomatrix gel to rat AVFs that were created using the femoral artery and vein of Sprague Dawley rats *via* end (vein) to side (artery) anastomosis. The fluorescent nanomatrix gel was created by the incorporation of an infrared fluorescent dye (IR Dye, LI-COR) to the PA molecule, and the dye fluorescence was observed using the Pearl imaging system (LI-COR) after gel implantation (Fig. 3f). Through the infrared imaging system, we found that the fluorescence of the perivascular nanomatrix gel gradually reduced over time, but was still detectable at 2 months (Supplementary Fig. S3). This result indicated that the applied nanomatrix gel degraded slowly and thus has the potential for prolonged release of NO during the AVF maturation process.

3.4. NO gel inhibits AVF intimal hyperplasia in rats.

The NO releasing nanomatrix gel (treatment group) or control gel without NO (control group) was applied directly over the venous anastomosis of the rat AVF (Fig. 4a–c; Supplementary video 1). At 7 days following AVF creation, the animal was euthanized and the AVF tissue was harvested to assess the early effects of the NO therapy on AVF maturation. Since the majority of stenosis and intimal formation in human AVF dysfunction occurs at the venous anastomosis, we analyzed the venous sections of our rat AVF anastomoses. The treatment group rats showed an approximately 70% reduction in the average intima/media area ratio at the venous anastomosis of the AVF compared to the control group, indicating that intimal hyperplasia development was significantly reduced with treatment of the NO releasing nanomatrix gel (Fig. 4d–f). The degree of stenosis at the venous anastomosis was also significantly reduced, which resulted in increased open lumen percentage in the treatment group compared to the control group (Supplementary Fig. S4).

These results were consistent with the reduction of venous intimal hyperplasia and stenosis in NOS3 OE mouse AVF models. Taken together, these results demonstrated the crucial role of NO on the regulation of venous intimal hyperplasia development at the AVF anastomosis.

3.5. NO gel increases cGMP and inhibits MCP-1 in rat AVFs.

We also assessed, using ELISA, whether our NO releasing nanomatrix gel can increase local AVF levels of cGMP, a vasodilation mediator. There was a 7-fold increase in cGMP levels in the treatment group compared to the control group at the venous anastomosis of the AVF (Fig. 4g); this trend was also observed when comparing NOS3 OE mice versus wild type mice (Fig. 2f). In addition, we analyzed the expression of inflammatory mediators (IL-1β and MCP-1) in the venous AVFs (Fig. 4h and i). IL-1β is known to be involved with vascular inflammation and remodeling [40]. However, there was no significant difference in IL-1β expression between the treatment and control groups in the venous AVFs. MCP-1 is one of the key cytokines regulating monocyte/macrophage infiltration and vascular smooth muscle cell proliferation, and it may also have important roles in promoting the development of intimal hyperplasia at the venous anastomosis of the AVFs [41]. MCP-1 expression was significantly reduced in the treatment group compared to the control group indicating that our NO gel therapy may reduce intimal hyperplasia by decreasing MCP-1 expression.

3.6. NO gel reduce α-SMA, Vimentin, Desmin and CD68 expression in rat AVFs.

Previous studies characterizing the cellular phenotypes with in the regions of intimal hyperplasia following AVF creation demonstrated the presence of α-SMA and Vimentin-positive myofibroblasts and Desmin-positive contractile smooth muscle cells [42, 43] and macrophages [44, 45]. Therefore in order to characterize the cellular phenotype in the outflow vein following NO therapy, we evaluated the expression of α-SMA, Vimentin, Desmin and CD68 within the intimal regions (Fig. 5). There was a significant reduction in the abundance of α-SMA, Vimentin and Desmin-expressing cells with in the intimal region with the NO gel treatment when compared to the control gel treatment ($p<0.05$). Furthermore, we observed a significantly lower number of CD68 (+) cells following NO gel therapy ($p<0.05$). Overall these results indicate there is a significant reduction in predominant intimal cell population following NO gel therapy when compared to the control gel therapy.

3.7. NO gel improves AVF hemodynamics in rats.

After its creation, the AVF undergoes vascular remodeling, with an increase in its lumen diameter being the desired outcome. A critical hemodynamic change triggering vascular remodeling, post-AVF creation, is the FWSS level. This immediate increase in blood flow has long been hypothesized to promote an adaptive response in the AVF in which the luminal diameter increases in an attempt to reduce FWSS to pre-AVF levels. Using MRI-based CFD approach on our rat AVF model, we evaluated venous AVF lumen area and hemodynamics of the NO releasing nanomatrix gel (treatment) and the control gel without NO (control) treated groups (Fig. 6; detailed procedures are described in Supporting Information). The venous AVF lumen cross-sectional area was significantly ($p<0.05$) larger in the treatment group (2.76 ± 0.65 mm^2) as compared to the control group (2.45 ± 0.44 mm^2) 7 days after AVF creation, suggesting that the NO releasing nanomatrix gel can

promote outward AVF remodeling (Fig. 7 a, b, and o). In addition, the treatment group had lower venous blood flow velocity and smoother streamlines compared to the control group (Fig. 7 c–f and p, Supplementary Videos 2–3). Thus, the treatment group showed lower FWSS and less vorticity compared to the control group, further suggesting that local NO releasing nanomatrix therapy may promote desired hemodynamic adaptation (Fig. 7 g–n, q, and r; Supplementary Videos 4–7).

3.8. Transcriptomics analysis of NO gel vs. control gel treated outflow AVF vein

We performed transcriptomic analysis using RNA-seq to identify potential changes in gene expression in NO gel treated AVF veins at 7 days. We sequenced an average 79 million reads per sample (range, 67–93 million reads), of which 55% (range, 48–59%) were uniquely aligned to the reference rat genome. We subsequently identified 1267 genes that were significantly differently expressed between NO gel treated AVF vein and control gel treated AVF vein using a 5% FDR. 511 genes were up-regulated and 756 significantly downregulated in the NO gel treated AVF veins (Supplemental Table 1). The log2 normalized counts from all 1267 significant genes were hierarchically clustered in the heatmap in Figure 8a.

We ran Ingenuity Pathway Analysis (IPA) to compare significant genes with its curated database of pathways and gene networks to predict which canonical pathways are activated (Z score of >0) and or inactivated (Z-score of <0). A total of 1190 significant genes were mapped to the IPA database and canonical pathways associated with inflammatory signaling, senescence (aging), and epithelial-mesenchymal transition were notably inactivated (Fig. 8b). Canonical pathways that were predicted to be activated included pathways in signal transduction that promotes metabolism, proliferation, cell survival, growth and angiogenesis (PI3K/AKT Signaling), and pathways that regulate transcription of target genes involved in energy metabolism, vascular function, oxidative stress, inflammation (PPARα/RXRα Activation) (Fig. 8b)(Supplemental Table 2).

Subsequently, we identified upstream regulators of NO gel treated AVF vein using IPA. Figure 8c demonstrates the top significantly activated and inactivated regulators and include multiple genes associated with cardiovascular remodeling. NO gel therapy inhibited many of these regulators predicted to be implicated in vascular remodeling such as TGFβ1, CCR2 (MCP-1), IL1B, and IL-6. Moreover, NO gel therapy activated regulators that influence TGFβ1 signaling (SMAD 7), inhibit smooth muscle cell proliferation (miR-455), and promote vessel dilation (NOS3)(Supplemental Table 3).

4. Discussion

Our present study demonstrated that local self-assembled NO releasing nanomatrix gel applied perivascularly on the AVF anastomosis can be an effective therapy to improve AVF maturation. The key findings from this study are that AVFs treated with NO releasing nanomatrix gel therapy when compared to control gel without NO: (1) inhibits venous intimal hyperplasia, (2) improves outward remodeling and hemodynamic adaptation, and (3) reduces AVF inflammation. Furthermore, we have demonstrated that the NO releasing gel degrades slowly over time, allowing the sustained release of the NO therapy. The animals

tolerated the NO releasing nanomatrix gel therapy well, and we did not observe any adverse responses.

Vascular access is the lifeline for the hemodialysis patient, as it is the conduit that allows for three times weekly dialysis treatment. The preferred vascular access is the AVF, and the United States vascular access guidelines recommend AVF placement in the majority of hemodialysis patients requiring vascular access [46–48]. Following surgical creation, AVFs require a maturation period to dilate and achieve sufficient blood flow for dialysis therapy, usually 6 weeks to 3 months. However, up to 60% of AVFs created never successfully mature for hemodialysis use (AVF maturation failure) due to intimal hyperplasia development and/or poor outward remodeling, particularly at the venous anastomosis of the AVF. This high maturation failure rate is currently the greatest barrier towards AVF use [42, 49, 50]. At present, there are no effective therapies to improve AVF maturation. The few therapies tested to date have largely focused on the delivery of antiplatelet (*e.g.*, aspirin, fish oil, and clopidogrel) and antiproliferative (*e.g.*, sirolimus and paclitaxel) agents, and have shown no benefit compared to placebo controls [51, 52]. These therapies have demonstrated high rates of AVF maturation failure likely due to the inability to locally deliver a sufficiently high dose of a drug in a sustained manner to the site of vascular injury, the AVF anastomosis. Additionally, various biomolecule candidates can be applied for improving vessel outward remodeling (e.g., prostaglandin, allicin, and TFG-β-activated protein kinase 1) or targeting “venous” intimal hyperplasia development (e.g., Resolvin D1 (RvD1), heparin, hyaluronic acid, and IL-4), but these compounds remain largely unexplored for AVF maturation [53–61]. Mechanisms leading to AVF maturation failure remain poorly understood. It has been hypothesized that poor hemodynamic and vascular biological responses after AVF creation result in venous intimal hyperplasia development and impaired outward remodeling [62–64]. NO is an important signaling molecule in the cardiovascular system. NO has many important properties, such as inhibition of platelet activity and smooth muscle cell proliferation and migration, reduction of inflammatory responses, and enhancement of endothelial cell proliferation [35, 65–67]. Based on these properties, NO has been known to inhibit intimal hyperplasia in arterial injury models [11, 12, 14]. Furthermore, NO is a potent vasodilator and plays an important role in vascular remodeling [67–69]. In our present study, we first demonstrated the important role of NOS3 in regulating AVF development by using NOS3 knockout and overexpression mice. Our results suggested that endothelial NO production is critical for inhibition of venous intimal hyperplasia and stimulation of a key vasodilatory mediator, cGMP, in the AVF. Thus, locally-delivered NO therapy that allows for sustained and controlled NO release may help mitigate venous intimal hyperplasia development and promote outward remodeling. Our rat studies supported this rationale.

Beneficial effects of perivascular NO delivery on inhibition of intimal hyperplasia have been previously demonstrated in arterial injury models [11–13]. However, there are only a handful of reports on NO therapy and venous intimal hyperplasia formation, where the vascular environment is different compared to arteries. Vein grafts and AVFs are the most common surgically created conduits that expose veins to the arterial environment. Thus, the long-term success of both of these conduits depends on the ability of the vein to adapt to the arterial hemodynamic conditions. Chaux *et al.* reported on delivering SPER/NO to

the external surface of vein grafts in hypercholesterolemic rabbits using a bio-degradable polymer, and observed a 39% reduction in vein graft hyperplasia at 28 days [70]. Fulton *et al.* reported on a local delivery of NO using a pluronic gel, which caused a 36% reduction in intimal hyperplasia formation in rabbit vein grafts at 28 days [71]. In our rat AVF study, we demonstrated that local delivery of NO inhibited venous intimal hyperplasia in an AVF setting by more than 70% when compared to the control. In addition, our results indicate that there is a significant reduction in previously known predominant intimal cell populations, that express α-SMA, vimentin, desmin and CD68, following NO gel therapy when compared to the control gel therapy. To the best of our knowledge, this study is the first report on the use of a local, perivascular delivered NO therapy on AVF with successful inhibition of venous intimal hyperplasia.

Local NO therapy appears to inhibit intimal hyperplasia through several mechanisms. Released NO may enhance endothelial cell proliferation at the site of vascular injury and restore the protective barrier. Previously reported studies have demonstrated that NO stimulated endothelial cell regeneration and thereby accelerated reendothelialization [72]. Another potential mechanism of intimal hyperplasia inhibition by NO, which we evaluated, may include the reduction of proinflammatory mediators such as MCP-1 (Fig. 4h). Previous studies in murine AVF models with genetic deficiency of MCP-1 demonstrated a marked reduction of intimal hyperplasia, reflected by the increased AVF patency at 6 weeks after creation [41]. Another previous studies showed that human stenotic AVF samples had increased MCP-1, which further indicated the importance of MCP-1 expression on AVF patency [73]. Our results from our western blot studies demonstrated a reduction in MCP-1 protein expression at the venous anastomosis, suggesting that reduction of inflammation may be a potential mechanism of our NO therapy to explain the reduction in intimal hyperplasia. Our results were also consistent with our *in vitro* studies, which demonstrated attenuation of inflammatory responses under dynamic flow [67].

To further understand the molecular pathways by which NO therapy mitigates intimal hyperplasia and promotes outward remodeling, we performed transcriptomic analysis using RNA-seq. We found that the majority of downregulated pathways from the NO therapy that are involved in signaling pathways related to inflammation, senescence (aging), and epithelial-mesenchymal transition were inactivated. This may play an important role in intimal hyperplasia development and outward remodeling. Moreover, we discovered the majority of upregulated pathways from the NO gel treatment involved pathways that regulate inflammation, vascular function, cell survival, and angiogenesis. Further analysis of upstream regulators demonstrated that upstream inflammatory regulators such as TGFβ1, CCR2 (receptor for MCP-1), IL1β, and IL-6 were inhibited by the NO gel treatment and regulators that influence TGFβ1 signaling (SMAD 7), inhibit smooth muscle cell proliferation (miR-455), and promote vessel dilation (NOS3) were activated by the NO gel treatment. This further supports our concept that NO gel therapy may promote successful AVF outward remodeling and inhibit intimal hyperplasia by suppressing proinflammatory responses and enhancing vasodilatory responses. In addition to our present study, two other animal studies evaluating locally applied therapies at the AVF outflow vein have also demonstrated attenuation of inflammation pathways using RNA-seq technology. Singh *et al.*, in a porcine AVF model, evaluated local delivery of 1a,25(OH)2D3 from poly(lactic-co-

glycolic acid) (PLGA) nanoparticles embedded in a thermosensitive Pluronic F127 hydrogel (1,25 NP) and demonstrated a decrease in signaling pathways associated with inflammation, apoptosis, and fibrosis [74]. Misra *et al.* created AVFs in mice with a humanized fractalkine receptor 1 (hCX3CR1) knocked in, with one group treated with an anti-hCX3CR1 VHH molecule applied at the outflow vein (KI-A) and a control group treated with a vehicle control (KI-V) [44]. RNA-seq analysis performed showed the KI-A treated group, as compared to the KI-V group, had decreased expression of inflammatory pathways and identified TNF-α and NF-kβ as potential targets of CX3CR1 inhibition.

In addition to inhibition of venous intimal hyperplasia, our results demonstrated the potential to enhance outward remodeling. Connection of a low-pressure vein to a high-pressure artery leads to a series of events that initiates an immediate increase in blood flow from the inflow artery into the outflow vein [62–64]. This rapid increase in flow results both in passive vascular distension and in NO synthesis by endothelial cells with subsequent vascular smooth muscle cell relaxation, resulting in acute vasodilation [62, 75–77]. A critically important post-AVF creation hemodynamic change triggering vascular wall remodeling is the FWSS [78–81], which is the frictional force exerted by blood flow on the vascular luminal surface. This increase in blood flow has long been hypothesized to provoke an adaptive response in the AVF in which the luminal diameter increases in an attempt to reduce FWSS to pre-AVF levels [80, 82]. Notably, AVFs treated with the NO releasing nanomatrix gel, as compared to AVFs with control gel administered, demonstrated increased vein area and lower FWSS and vorticity at 7 days after creation, suggesting improved hemodynamic adaptation (Fig. 6). Furthermore, AVFs treated with the NO releasing nanomatrix gel also increased AVF vein cGMP levels, suggesting that our local NO delivery may also have the potential to positively enhance smooth muscle cell relaxation, another mechanism to promote outward remodeling.

Our self-assembled nanomatrix technology and delivery system have several key advantages in the setting of improving maturation. First, the release kinetics of NO from the nanomatrix showed an initial burst release followed by slow, sustained delivery over an extended duration, thus ideally targeting critical periods of AVF remodeling and development. Immediate release of NO is critical to promote vasodilation, while sustained release is important to promote outward remodeling and inhibit intimal hyperplasia development over time. Second, our novel therapy utilizes a gel to deliver NO *via* a perivascular route. NO is a freely diffusible molecule and can penetrate all layers of the blood vessel (*e.g.*, adventitia, media, and intima). This perivascular approach may be advantageous because (a) applying NO directly to the adventitia (“outside-in approach”) may be far more effective in blocking adventitial activation and fibroblast migration, and (b) direct local application of a small amount of drug can result in high concentrations at the site of vascular injury (venous anastomosis) with minimal systemic toxicity. Third, properties of the nanomatrix gel are beneficial for therapeutic NO delivery to the AVF: (a) PA molecules can self-assemble into the nanomatrix gel for NO release without further modification, such as chemical conjugation or photo cross-linking [15], that may have undesired complications. (b) The gelation properties can be tunable by co-assembling various PAs, which allows maintenance of gel stability during AVF maturation [16]. (c) Slow degradation of the nanomatrix gel through the enzyme-mediated degradation sequence (MMP-2 degradable site) provides

sustained release of NO [17]. Our degradation studies confirmed slow degradation over a two-month period, an optimal window for continuous release of NO during the AVF development period.

Our study has several limitations. First, in this study, we have focused specifically on the effects of our NO releasing nanomatrix gel on early (*i.e.*, 7 days) AVF remodeling and intimal hyperplasia development. Within the first week, we observed significant intimal hyperplasia development. Additionally, other studies showed that cell proliferation, which contributes to the formation of intimal hyperplasia, tends to occur at an early timepoint reaching a maximum at day 5, when changes in blood flow and diameter are greatest [83, 84]. Therefore, therapeutic efficacy is important at the early timepoint in the prevention of intimal hyperplasia. An early time point observation is also important to determine clinical AVF outcomes. The increases in blood flow and vessel diameter occurs soon after AVF creation in a great majority of clinical cases [50, 78, 85–89]. Blood flow reaches higher than minimum blood flow rate ≥ 500 ml / min for adequate AVF development for dialysis use within 1 day and it is critical for predicting AVF maturation within two weeks [50, 78, 85–91]. Therefore, demonstrating efficacy at 1 week powerfully predicts successful AVF maturation. A second limitation is that our study was performed in healthy rodents. AVFs are created in humans in the setting of advanced chronic kidney disease, so we must remain cautious in extrapolating results from rodents with healthy kidneys to patients with advanced chronic kidney disease where baseline levels of endothelial dysfunction, oxidative stress, and inflammation may be increased. Future studies to investigate the efficacy and safety of the NO gel therapy in animals with kidney disease and for durations longer than 7 days are warranted.

For our future Food and Drug Administration (FDA) application, we plan to perform comprehensive biocompatibility testing of our gel by following the guidelines from International Organization for Standardization (ISO). Our previous studies successfully demonstrated the biocompatibility of various PA nanomatrix gel applications *in vitro* and *in vivo* models including mouse, rat, and dog [92–94]. We did not observe any scar tissue formation, foreign body response, or physiological changes in any of animal model. Further biocompatibility testing will be performed including evaluation of cytotoxicity, intracutaneous reactivity, sensitization, systemic toxicity, pyrogenicity, genotoxicity, and local effects under good laboratory practice (GLP) conditions as required by the FDA.

5. Conclusion

AVF is the most common vascular access method for hemodialysis treatment, but frequent failures (60%) of AVF maturation, due to early intimal hyperplasia development and poor outward remodeling, create a large financial cost and reduce quality of life. In this study, we demonstrated that the perivascular application of NO releasing nanomatrix gel to the anastomosis after AVF creation significantly reduces venous intimal hyperplasia development and enhances outward vascular remodeling by increasing vasodilation and improving hemodynamic adaptation. Furthermore, the NO releasing nanomatrix gel therapy also reduces local inflammation at the AVF-vein anastomosis. Our results suggest that our novel NO releasing nanomatrix delivered perivascularly *via* gel application has the potential

to mitigate AVF maturation failure. As a future study, we will apply the NO releasing nanomatrix gel to a large animal AVF model, which is more closely related to human physiology for clinical setting.

Supplementary Material

Refer to Web version on PubMed Central for supplementary material.

Acknowledgements

This work was supported by National Institutes of Health (NIH) Grants R43DK109789 (Co-PI: Timmy Lee & Patrick Hwang), R44DK109789-03 & -04 (Co-PI: Timmy Lee & Patrick Hwang), R01HL139692 and 1R01HL153244 (PI: Timmy Lee), and R01HL125391 (PI: Ho-Wook Jun), Department of Veterans Affairs Merit Award I01BX003387 (PI: Timmy Lee), and Alabama Research and Development Enhancement Fund 1ARDEF22 09 (PI: Ho-Wook Jun). Yan-Ting Shiu is supported by NIH Grants R01DK100505, R01DK121227, and Department of Veterans Affairs Merit Award I01BX004133.

MRI imaging was performed at the UAB Small Imaging Facility Core supported by the Comprehensive Cancer Center Preclinical Imaging Shared Facility Grant P30CA013148. Murine AVFs were created in the University of Alabama at Birmingham George M. O'Brien Kidney Research Center (P30DK079337) pre-clinical studies core.

Research reported in this publication utilized the informatics Shared Resource at Huntsman Cancer Institute at the University of Utah and was supported by the National Cancer Institute of the National Institutes of Health Award P30CA042014.

Data availability statement

The data that support the findings of this study are available from the corresponding author (s), TL and HWJ, upon reasonable request.

References

[1]. Saran R, Li Y, Robinson B, Abbott KC, Agodoa LY, et al. , US Renal Data System 2015 Annual Data Report: Epidemiology of Kidney Disease in the United States, Am. J. Kidney Dis. 67 (3 Suppl 1) (2016) Svii, S1–305.

[2]. Feldman HI, Held PJ, Hutchinson JT, Stoiber E, Hartigan MF, et al. , Hemodialysis vascular access morbidity in the United States, Kidney. Int. 43 (5) (1993) 1091–6. [PubMed: 8510387]

[3]. Allon M, Robbin ML, Increasing arteriovenous fistulas in hemodialysis patients: problems and solutions, Kidney. Int. 62 (4) (2002) 1109–24. [PubMed: 12234281]

[4]. Feldman HI, Kobrin S, Wasserstein A, Hemodialysis vascular access morbidity, J. Am. Soc. Nephrol. 7 (4) (1996) 523–35. [PubMed: 8724885]

[5]. Furchgott RF, Role of endothelium in responses of vascular smooth muscle, Circ. Res. 53 (5) (1983) 557–73. [PubMed: 6313250]

[6]. Furchgott RF, Zawadzki JV, The obligatory role of endothelial cells in the relaxation of arterial smooth muscle by acetylcholine, Nature 288 (5789) (1980) 373–6. [PubMed: 6253831]

[7]. Garg UC, Hassid A, Nitric oxide-generating vasodilators and 8-bromo-cyclic guanosine monophosphate inhibit mitogenesis and proliferation of cultured rat vascular smooth muscle cells, J. Clin. Invest. 83 (5) (1989) 1774–7. [PubMed: 2540223]

[8]. Kubes P, Suzuki M, Granger DN, Nitric oxide: an endogenous modulator of leukocyte adhesion, Proc. Natl. Acad. Sci. U. S. A. 88 (11) (1991) 4651–5. [PubMed: 1675786]

[9]. Radomski MW, Palmer RM, Moncada S, The role of nitric oxide and cGMP in platelet adhesion to vascular endothelium, Biochem. Biophys. Res. Commun. 148 (3) (1987) 1482–9. [PubMed: 2825688]

[10]. Radomski MW, Palmer RM, Moncada S, Endogenous nitric oxide inhibits human platelet adhesion to vascular endothelium, Lancet 2 (8567) (1987) 1057–8. [PubMed: 2889967]

[11]. Havelka GE, Moreira ES, Rodriguez MP, Tsihlis ND, Wang Z, et al. , Nitric oxide delivery via a permeable balloon catheter inhibits neointimal growth after arterial injury, J. Surg. Res. 180 (1) (2013) 35–42. [PubMed: 23164361]

[12]. Pearce CG, Najjar SF, Kapadia MR, Murar J, Eng J, et al. , Beneficial effect of a short-acting NO donor for the prevention of neointimal hyperplasia, Free Radic. Biol. Med. 44 (1) (2008) 73–81. [PubMed: 18045549]

[13]. Bahnson ES, Vavra AK, Flynn ME, Vercammen JM, Jiang Q, et al. , Long-term effect of PROLI/NO on cellular proliferation and phenotype after arterial injury, Free Radic. Biol. Med. 90 (2016) 272–86. [PubMed: 26627935]

[14]. Bahnson ES, Koo N, Cantu-Medellin N, Tsui AY, Havelka GE, et al. , Nitric oxide inhibits neointimal hyperplasia following vascular injury via differential, cell-specific modulation of SOD-1 in the arterial wall, Nitric Oxide 44 (2015) 8–17. [PubMed: 25460325]

[15]. Jun HW, Yuwono V, Paramonov SE, Hartgerink JD, Enzyme-mediated degradation of peptide-amphiphile nanofiber networks, Adv. Mater. 17 (2005) 2612–2617.

[16]. Anderson JM, Andukuri A, Lim D, Jun HW, Modulating the gelation properties of self-assembling peptide amphiphiles, ACS Nano 9 (2009) 3447–3454.

[17]. Kushwaha M, Anderson JM, Bosworth CA, Andukuri A, Minor WP, et al. , A nitric oxide releasing, self assembled peptide amphiphile matrix that mimics native endothelium for coating implantable cardiovascular devices, Biomaterials 31 (7) (2010) 1502–8. [PubMed: 19913295]

[18]. Jun HW, Taite LJ, West JL, Nitric oxide-producing polyurethanes, Biomacromolecules 6 (2) (2005) 838–44. [PubMed: 15762649]

[19]. Jones SP, Greer JJ, van Haperen R, Duncker DJ, de Crom R, et al. , Endothelial nitric oxide synthase overexpression attenuates congestive heart failure in mice, Proc. Natl. Acad. Sci. U. S. A. 100 (8) (2003) 4891–6. [PubMed: 12676984]

[20]. Jones SP, Greer JJ, Kakkar AK, Ware PD, Turnage RH, et al. , Endothelial nitric oxide synthase overexpression attenuates myocardial reperfusion injury, Am. J. Physiol. Heart. Circ. Physiol. 286 (1) (2004) H276–82. [PubMed: 12969888]

[21]. Pike D, Shiu YT, Cho YF, Le H, Somarathna M, et al. , The effect of endothelial nitric oxide synthase on the hemodynamics and wall mechanics in murine arteriovenous fistulas, Sci. Rep. 9 (1) (2019) 4299. [PubMed: 30862797]

[22]. Pike D, Shiu YT, Somarathna M, Guo L, Isayeva T, et al. , High resolution hemodynamic profiling of murine arteriovenous fistula using magnetic resonance imaging and computational fluid dynamics, Theor. Biol. Med. Model. 14 (1) (2017) 5. [PubMed: 28320412]

[23]. Andukuri A, Kushwaha M, Tambralli A, Anderson JM, Dean DR, et al. , A hybrid biomimetic nanomatrix composed of electrospun polycaprolactone and bioactive peptide amphiphiles for cardiovascular implants, Acta Biomater. 7 (1) (2011) 225–33. [PubMed: 20728588]

[24]. Andukuri A, Min I, Hwang P, Alexander G, Marshall LE, et al. , Evaluation of the effect of expansion and shear stress on a self-assembled endothelium mimicking nanomatrix coating for drug eluting stents in vitro and in vivo, Biofabrication 6 (3) (2014) 035019. [PubMed: 25048693]

[25]. Lee T, Chauhan V, Krishnamoorthy M, Wang Y, Arend L, et al. , Severe venous neointimal hyperplasia prior to dialysis access surgery, Nephrol. Dial. Transplant. 26 (7) (2011) 2264–70. [PubMed: 21220751]

[26]. Lee T, Somarathna M, Hura A, Wang Y, Campos B, et al. , Natural history of venous morphologic changes in dialysis access stenosis, J. Vasc. Access. 15 (4) (2014) 298–305. [PubMed: 24500849]

[27]. Dobin A, Davis CA, Schlesinger F, Drenkow J, Zaleski C, et al. , STAR: ultrafast universal RNA-seq aligner, Bioinformatics 29 (1) (2013) 15–21. [PubMed: 23104886]

[28]. Martin M, Cutadapt removes adapter sequences from high-throughput sequencing reads, 2011 17 (1) (2011) 3.

[29]. Liao Y, Smyth GK, Shi W, featureCounts: an efficient general purpose program for assigning sequence reads to genomic features, Bioinformatics 30 (7) (2014) 923–30. [PubMed: 24227677]

[30]. Ewels P, Magnusson M, Lundin S, Kaller M, MultiQC: summarize analysis results for multiple tools and samples in a single report, Bioinformatics 32 (19) (2016) 3047–8. [PubMed: 27312411]

[31]. Love MI, Huber W, Anders S, Moderated estimation of fold change and dispersion for RNA-seq data with DESeq2, Genome Biology 15 (12) (2014) 550. [PubMed: 25516281]

[32]. Kramer A, Green J, Pollard J Jr., Tugendreich S, Causal analysis approaches in Ingenuity Pathway Analysis, Bioinformatics 30 (4) (2014) 523–30. [PubMed: 24336805]

[33]. Krawutschke C, Koesling D, Russwurm M, Cyclic GMP in Vascular Relaxation: Export Is of Similar Importance as Degradation, Arterioscler. Thromb. Vasc. Biol. 35 (9) (2015) 2011–9. [PubMed: 26205960]

[34]. Furchgott RF, Endothelium-derived relaxing factor: discovery, early studies, and identification as nitric oxide, Biosci. Rep. 19 (4) (1999) 235–51. [PubMed: 10589989]

[35]. Alexander GC, Hwang PTJ, Chen J, Kim J, Brott BC, et al. , Nanomatrix Coated Stent Enhances Endothelialization but Reduces Platelet, Smooth Muscle Cell, and Monocyte Adhesion under Physiologic Conditions, ACS Biomater. Sci. Eng. 4 (1) (2018) 107–115. [PubMed: 31538110]

[36]. Mezger TG, The Rheology Handbook: for Users of Rotational and Oscillatory Rheometers, 2 ed., Vincentz Network, Hanover, Germany, 2006.

[37]. Li H, Jen S, Ramayya T, Bowers HG, Rotem E, Unanticipated late maturation of an arteriovenous fistula after creation of separate graft access, Quant. Imaging Med. Surg. 8 (4) (2018) 444–446. [PubMed: 29928609]

[38]. Cheung AK, Imrey PB, Alpers CE, Robbin ML, Radeva M, et al. , Intimal Hyperplasia, Stenosis, and Arteriovenous Fistula Maturation Failure in the Hemodialysis Fistula Maturation Study, J. Am. Soc. Nephrol. 28 (10) (2017) 3005–3013. [PubMed: 28710091]

[39]. Brunori G, Ravani P, Mandolfo S, Imbasciati E, Malberti F, et al. , Fistula maturation: doesn't time matter at all?, Nephrol. Dial. Transplant. 20 (4) (2005) 684–7. [PubMed: 15772262]

[40]. Li P, Li YL, Li ZY, Wu YN, Zhang CC, et al. , Cross talk between vascular smooth muscle cells and monocytes through interleukin-1beta/interleukin-18 signaling promotes vein graft thickening, Arterioscler. Thromb. Vasc. Biol. 34 (9) (2014) 2001–11. [PubMed: 25012128]

[41]. Juncos JP, Grande JP, Kang L, Ackerman AW, Croatt AJ, et al. , MCP-1 contributes to arteriovenous fistula failure, J. Am. Soc. Nephrol. 22 (1) (2011) 43–8. [PubMed: 21115617]

[42]. Roy-Chaudhury P, Arend L, Zhang J, Krishnamoorthy M, Wang Y, et al. , Neointimal hyperplasia in early arteriovenous fistula failure, Am. J. Kidney Dis. 50 (5) (2007) 782–90. [PubMed: 17954291]

[43]. Alpers CE, Imrey PB, Hudkins KL, Wietecha TA, Radeva M, et al. , Histopathology of Veins Obtained at Hemodialysis Arteriovenous Fistula Creation Surgery, J Am Soc Nephrol 28 (10) (2017) 3076–3088. [PubMed: 28724774]

[44]. Misra S, Kilari S, Yang B, Sharma A, Wu CC, et al. , Anti Human CX3CR1 VHH Molecule Attenuates Venous Neointimal Hyperplasia of Arteriovenous Fistula in Mouse Model, J Am Soc Nephrol (2021).

[45]. Brahmbhatt A, Remuzzi A, Franzoni M, Misra S, The molecular mechanisms of hemodialysis vascular access failure, Kidney Int 89 (2) (2016) 303–316. [PubMed: 26806833]

[46]. Shiu YT, Rotmans JI, Geelhoed WJ, Pike DB, Lee T, Arteriovenous conduits for hemodialysis: how to better modulate the pathophysiological vascular response to optimize vascular access durability, Am. J. Physiol. Renal. Physiol 316 (5) (2019) F794–F806. [PubMed: 30785348]

[47]. Santoro D, Benedetto F, Mondello P, Pipito N, Barilla D, et al. , Vascular access for hemodialysis: current perspectives, Int. J. Nephrol. Renovasc. Dis. 7 (2014) 281–94. [PubMed: 25045278]

[48]. MacRae JM, Oliver M, Clark E, Dipchand C, Hiremath S, et al. , Arteriovenous Vascular Access Selection and Evaluation, Can. J. Kidney Health Dis. 3 (2016) 1–13. [PubMed: 26767116]

[49]. Duque JC, Tabbara M, Martinez L, Cardona J, Vazquez-Padron RI, et al. , Dialysis Arteriovenous Fistula Failure and Angioplasty: Intimal Hyperplasia and Other Causes of Access Failure, Am. J. Kidney. Dis. 69 (1) (2017) 147–151. [PubMed: 28084215]

[50]. Asif A, Roy-Chaudhury P, Beathard GA, Early arteriovenous fistula failure: a logical proposal for when and how to intervene, Clin. J. Am. Soc. Nephrol. 1 (2) (2006) 332–9.

[51]. Dember LM, Beck GJ, Allon M, Delmez JA, Dixon BS, et al. , Effect of clopidogrel on early failure of arteriovenous fistulas for hemodialysis: a randomized controlled trial, JAMA 299 (18) (2008) 2164–71. [PubMed: 18477783]

[52]. Irish AB, Viecelli AK, Hawley CM, Hooi LS, Pascoe EM, et al. , Effect of Fish Oil Supplementation and Aspirin Use on Arteriovenous Fistula Failure in Patients Requiring Hemodialysis: A Randomized Clinical Trial, JAMA Intern. Med. 177 (2) (2017) 184–193. [PubMed: 28055065]

[53]. P. Franchin M, G, Castelli P, and Tozzi M, Initial experience with analogues of prostaglandins for hemodialysis access induced distal ischemia, J. Vasc. Endovasc. Surg 1 (3) (2016) 8.

[54]. Garcia-Trejo EM, Arellano-Buendia AS, Arguello-Garcia R, Loredo-Mendoza ML, Garcia-Arroyo FE, et al. , Effects of Allicin on Hypertension and Cardiac Function in Chronic Kidney Disease, Oxid Med Cell Longev 2016 (2016) 3850402. [PubMed: 27990229]

[55]. Hu H, Lee SR, Bai H, Guo J, Hashimoto T, et al. , TGFbeta (Transforming Growth Factor-Beta)-Activated Kinase 1 Regulates Arteriovenous Fistula Maturation, Arterioscler Thromb Vasc Biol 40 (7) (2020) e203–e213. [PubMed: 32460580]

[56]. Wu B, Mottola G, Chatterjee A, Lance KD, Chen M, et al. , Perivascular delivery of resolvin D1 inhibits neointimal hyperplasia in a rat model of arterial injury, J Vasc Surg 65 (1) (2017) 207–217 e3. [PubMed: 27034112]

[57]. Wu B, Werlin EC, Chen M, Mottola G, Chatterjee A, et al. , Perivascular delivery of resolvin D1 inhibits neointimal hyperplasia in a rabbit vein graft model, J Vasc Surg 68 (6S) (2018) 188S–200S e4. [PubMed: 30064835]

[58]. Edelman ER, Nathan A, Katada M, Gates J, Karnovsky MJ, Perivascular graft heparin delivery using biodegradable polymer wraps, Biomaterials 21 (22) (2000) 2279–86. [PubMed: 11026634]

[59]. Freeman J, Chen A, Weinberg RJ, Okada T, Chen C, et al. , Sustained Thromboresistant Bioactivity with Reduced Intimal Hyperplasia of Heparin-Bonded Polytetrafluoroethylene Propaten Graft in a Chronic Canine Femoral Artery Bypass Model, Ann Vasc Surg 49 (2018) 295–303. [PubMed: 29197605]

[60]. Chajara A, Raoudi M, Delpech B, Levesque H, Inhibition of arterial cells proliferation in vivo in injured arteries by hyaluronan fragments, Atherosclerosis 171 (1) (2003) 15–19. [PubMed: 14642401]

[61]. Tan RP, Chan AHP, Wei S, Santos M, Lee BSL, et al. , Bioactive Materials Facilitating Targeted Local Modulation of Inflammation, JACC Basic Transl Sci 4 (1) (2019) 56–71. [PubMed: 30847420]

[62]. Rothuizen TC, Wong C, Quax PH, van Zonneveld AJ, Rabelink TJ, et al. , Arteriovenous access failure: more than just intimal hyperplasia?, Nephrol. Dial. Transplant. 28 (5) (2013) 1085–92. [PubMed: 23543595]

[63]. Lee T, Novel paradigms for dialysis vascular access: downstream vascular biology--is there a final common pathway?, Clin. J. Am. Soc. Nephrol. 8 (12) (2013) 2194–201.

[64]. Lee T, Misra S, New Insights into Dialysis Vascular Access: Molecular Targets in Arteriovenous Fistula and Arteriovenous Graft Failure and Their Potential to Improve Vascular Access Outcomes, Clin. J. Am. Soc. Nephrol. 11 (8) (2016) 1504–12.

[65]. Kuo PC, Schroeder RA, The emerging multifaceted roles of nitric oxide, Ann. Surg. 221 (3) (1995) 220–35. [PubMed: 7717775]

[66]. Sneddon JM, Vane JR, Endothelium-derived relaxing factor reduces platelet adhesion to bovine endothelial cells, Proc. Natl. Acad. Sci. U. S. A. 85 (8) (1988) 2800–4. [PubMed: 3258664]

[67]. Alexander GC, Vines JB, Hwang P, Kim T, Kim JA, et al. , Novel Multifunctional Nanomatrix Reduces Inflammation in Dynamic Conditions in Vitro and Dilates Arteries ex Vivo, ACS Appl. Mater. Interfaces 8 (8) (2016) 5178–87. [PubMed: 26849167]

[68]. Rudic RD, Shesely EG, Maeda N, Smithies O, Segal SS, et al. , Direct evidence for the importance of endothelium-derived nitric oxide in vascular remodeling, J. Clin. Invest. 101 (4) (1998) 731–6. [PubMed: 9466966]

[69]. Schleicher M, Sessa WC, Are the mechanisms for NO-dependent vascular remodeling different from vasorelaxation in vivo?, Arterioscler. Thromb. Vasc. Biol. 28 (7) (2008) 1207–8. [PubMed: 18565841]

[70]. Chaux A, Ruan XM, Fishbein MC, Ouyang Y, Kaul S, et al. , Perivascular delivery of a nitric oxide donor inhibits neointimal hyperplasia in vein grafts implanted in the arterial circulation, J. Thorac. Cardiovasc. Surg 115 (3) (1998) 604–12; discussion 612–4. [PubMed: 9535448]

[71]. Fulton GJ, Davies MG, Barber L, Gray JL, Svendsen E, et al. , Local effects of nitric oxide supplementation and suppression in the development of intimal hyperplasia in experimental vein grafts, Eur. J. Vasc. Endovasc. Surg. 15 (4) (1998) 279–89. [PubMed: 9610339]

[72]. Guo JP, Panday MM, Consigny PM, Lefer AM, Mechanisms of vascular preservation by a novel NO donor following rat carotid artery intimal injury, Am. J. Physiol. 269 (3 Pt 2) (1995) H1122–31. [PubMed: 7573510]

[73]. Liu BC, Li L, Gao M, Wang YL, Yu JR, Microinflammation is involved in the dysfunction of arteriovenous fistula in patients with maintenance hemodialysis, Chin Med J (Engl) 121 (21) (2008) 2157–61. [PubMed: 19080177]

[74]. Singh AK, Cai C, Kilari S, Zhao C, Simeon ML, et al. , 1alpha,25-Dihydroxyvitamin D3 Encapsulated in Nanoparticles Prevents Venous Neointimal Hyperplasia and Stenosis in Porcine Arteriovenous Fistulas, J Am Soc Nephrol (2021).

[75]. Moncada S, Higgs A, The L-arginine-nitric oxide pathway, N. Engl. J. Med. 329 (27) (1993) 2002–12. [PubMed: 7504210]

[76]. Cooke JP, Rossitch E Jr., Andon NA, Loscalzo J, Dzau VJ, Flow activates an endothelial potassium channel to release an endogenous nitrovasodilator, J. Clin. Invest. 88 (5) (1991) 1663–71. [PubMed: 1719029]

[77]. Tronc F, Wassef M, Esposito B, Henrion D, Glagov S, et al. , Role of NO in flow-induced remodeling of the rabbit common carotid artery, Arterioscler. Thromb. Vasc. Biol. 16 (10) (1996) 1256–62. [PubMed: 8857922]

[78]. Corpataux JM, Haesler E, Silacci P, Ris HB, Hayoz D, Low-pressure environment and remodelling of the forearm vein in Brescia-Cimino haemodialysis access, Nephrol. Dial. Transplant 17 (6) (2002) 1057–62. [PubMed: 12032197]

[79]. Ben Driss A, Benessiano J, Poitevin P, Levy BI, Michel JB, Arterial expansive remodeling induced by high flow rates, Am. J. Physiol. 272 (2 Pt 2) (1997) H851–8. [PubMed: 9124448]

[80]. Girerd X, London G, Boutouyrie P, Mourad JJ, Safar M, et al. , Remodeling of the radial artery in response to a chronic increase in shear stress, Hypertension 27 (3 Pt 2) (1996) 799–803. [PubMed: 8613243]

[81]. Kamiya A, Togawa T, Adaptive regulation of wall shear stress to flow change in the canine carotid artery, Am. J. Physiol. 239 (1) (1980) H14–21. [PubMed: 7396013]

[82]. Ene-Iordache B, Mosconi L, Antiga L, Bruno S, Anghileri A, et al. , Radial artery remodeling in response to shear stress increase within arteriovenous fistula for hemodialysis access, Endothelium 10 (2) (2003) 95–102. [PubMed: 12791517]

[83]. Kalra M, Miller VM, Early remodeling of saphenous vein grafts: proliferation, migration and apoptosis of adventitial and medial cells occur simultaneously with changes in graft diameter and blood flow, J Vasc Res 37 (6) (2000) 576–84. [PubMed: 11146412]

[84]. Dilley RJ, McGeachie JK, Tennant M, The role of cell proliferation and migration in the development of a neo-intimal layer in veins grafted into arteries, in rats, Cell Tissue Res 269 (2) (1992) 281–7. [PubMed: 1423495]

[85]. Won T, Jang JW, Lee S, Han JJ, Park YS, et al. , Effects of intraoperative blood flow on the early patency of radiocephalic fistulas, Ann Vasc Surg 14 (5) (2000) 468–72. [PubMed: 10990556]

[86]. Tordoir JH, Rooyens P, Dammers R, van der Sande FM, de Haan M, et al. , Prospective evaluation of failure modes in autogenous radiocephalic wrist access for haemodialysis, Nephrol Dial Transplant 18 (2) (2003) 378–83. [PubMed: 12543895]

[87]. Yerdel MA, Kesenci M, Yazicioglu KM, Doseyen Z, Turkcapar AG, et al. , Effect of haemodynamic variables on surgically created arteriovenous fistula flow, Nephrol Dial Transplant 12 (8) (1997) 1684–8. [PubMed: 9269649]

[88]. Lin SL, Chen HS, Huang CH, Yen TS, Predicting the outcome of hemodialysis arteriovenous fistulae using duplex ultrasonography, J Formos Med Assoc 96 (11) (1997) 864–8. [PubMed: 9409117]

[89]. Robbin ML, Chamberlain NE, Lockhart ME, Gallichio MH, Young CJ, et al. , Hemodialysis arteriovenous fistula maturity: US evaluation, Radiology 225 (1) (2002) 59–64. [PubMed: 12354984]

[90]. Robbin ML, Greene T, Cheung AK, Allon M, Berceli SA, et al. , Arteriovenous Fistula Development in the First 6 Weeks after Creation, Radiology 279 (2) (2016) 620–9. [PubMed: 26694050]

[91]. Robbin ML, Greene T, Allon M, Dember LM, Imrey PB, et al. , Prediction of Arteriovenous Fistula Clinical Maturation from Postoperative Ultrasound Measurements: Findings from the Hemodialysis Fistula Maturation Study, J Am Soc Nephrol 29 (11) (2018) 2735–2744. [PubMed: 30309898]

[92]. Ban K, Park HJ, Kim S, Andukuri A, Cho KW, et al. , Cell therapy with embryonic stem cell-derived cardiomyocytes encapsulated in injectable nanomatrix gel enhances cell engraftment and promotes cardiac repair, ACS Nano 8 (10) (2014) 10815–25. [PubMed: 25210842]

[93]. Anderson J, Patterson J, Vines J, Javed A, Gilbert S, et al. , Biphasic Peptide Amphiphile Nanomatrix Embedded with Hydroxyapatite Nanoparticles for Stimulated Osteoinductive Response, ACS Nano 5 (2011) 9463–9479. [PubMed: 22077993]

[94]. Moon CY, Nam OH, Kim M, Lee HS, Kaushik SN, et al. , Effects of the nitric oxide releasing biomimetic nanomatrix gel on pulp-dentin regeneration: Pilot study, PLoS One 13 (10) (2018) e0205534. [PubMed: 30308037]

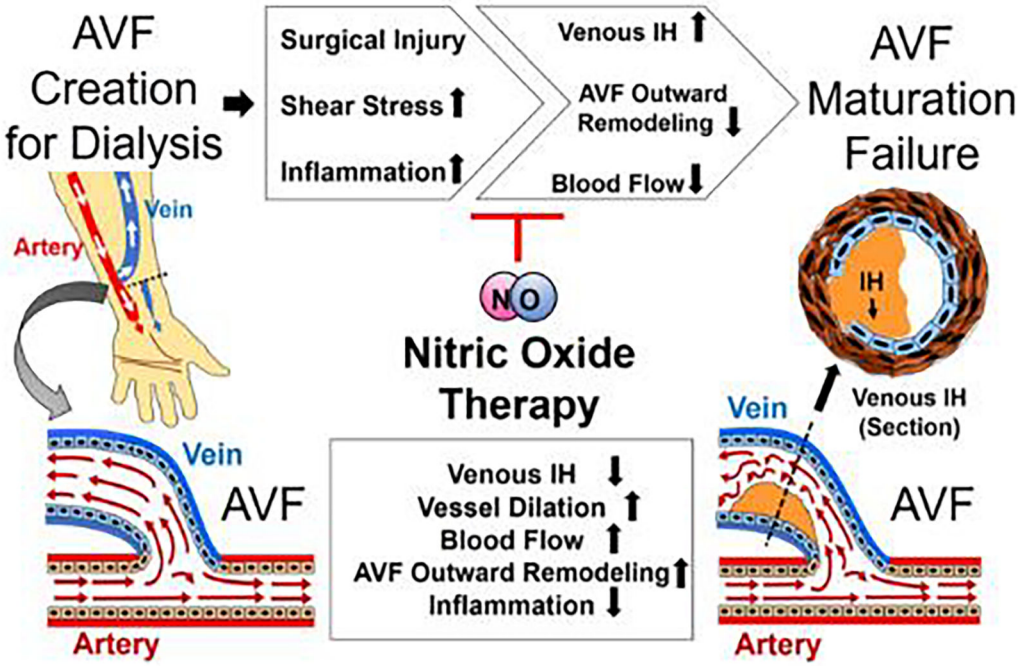

Fig. 1. AVF maturation failure and NO therapy.

Progress of AVF maturation failure after AVF creation and potential application of NO therapy to improve AVF maturation process for hemodialysis. IH: Intimal hyperplasia.

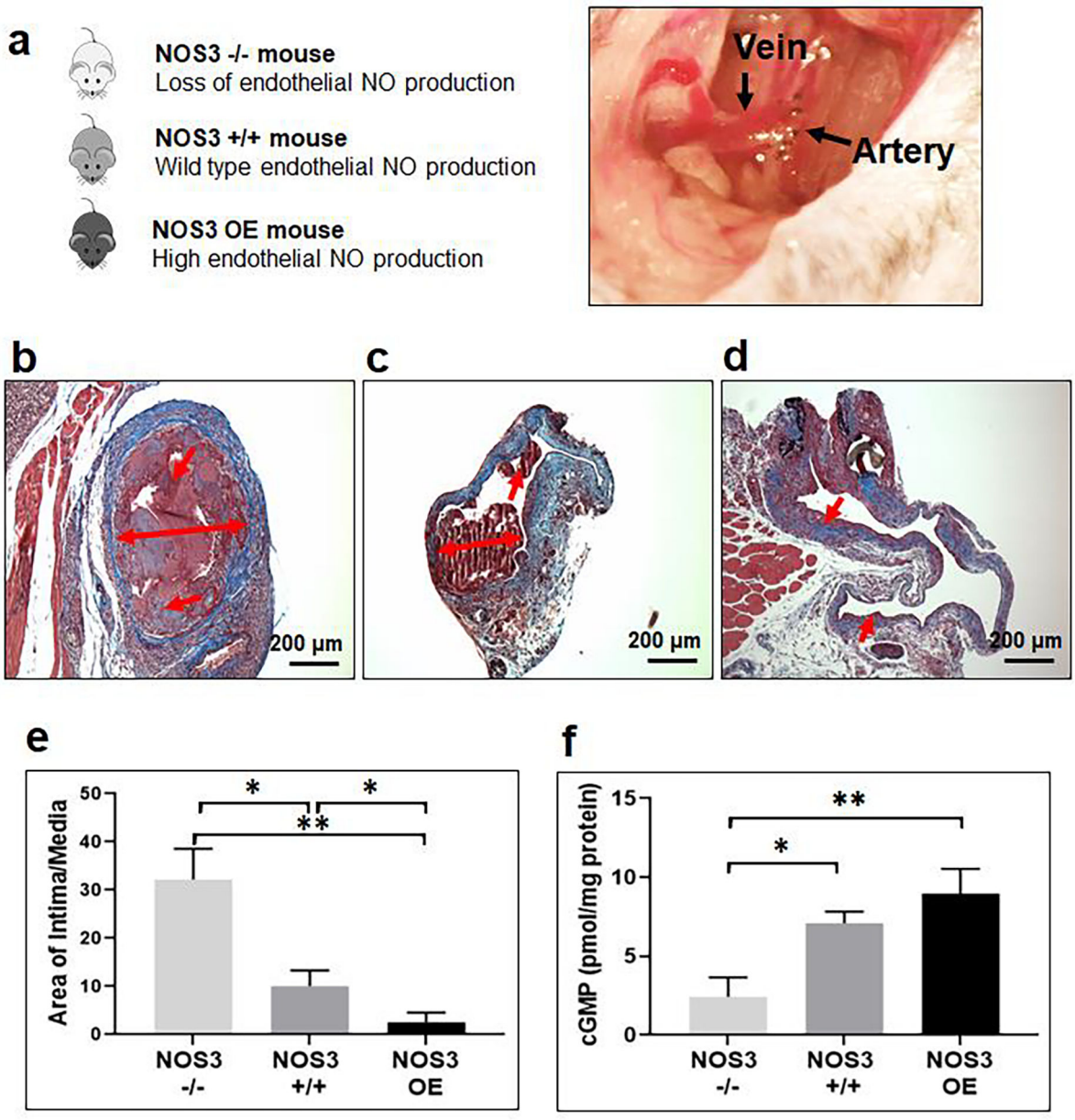

Fig. 2. Effects of differential NOS3 expression on biological response at 7 days in murine AVF.

(**a**) Murine jugular (end) vein to carotid artery (side) AVF model and the different genotypes used in this study. Mouse strains: NOS3−/− (knockout), NOS3+/+ (wild type), and NOS3 OE (overexpression). Representative histological images of venous intimal hyperplasia development following 7 days post AVF creation in (**b**) NOS3−/−, (**c**) NOS3+/+, and (**d**) NOS3 OE mice. Note the level of severe intimal hyperplasia formation in the NOS3−/− mouse and the restricted intimal hyperplasia formation with NOS3 OE. Single and double-headed arrows: Intimal hyperplasia development. (**e**) Morphometric analysis from AVF veins. Data are presented as the mean ± s.e.m. (n=3 for NOS3−/− group and n=4 for NOS3−/− and NOS3 OE groups). *p<0.05 and **p<0.01. (**f**) cGMP concentration in AVF veins measured using ELISA. Data are presented as the mean ± s.e.m. (n=3 for NOS3+/+

mice group and n=4 for NOS3−/− and NOS3 OE mice groups). *p<0.05 and **p<0.01. An unpaired t-test was used to test for statistical differences between groups.

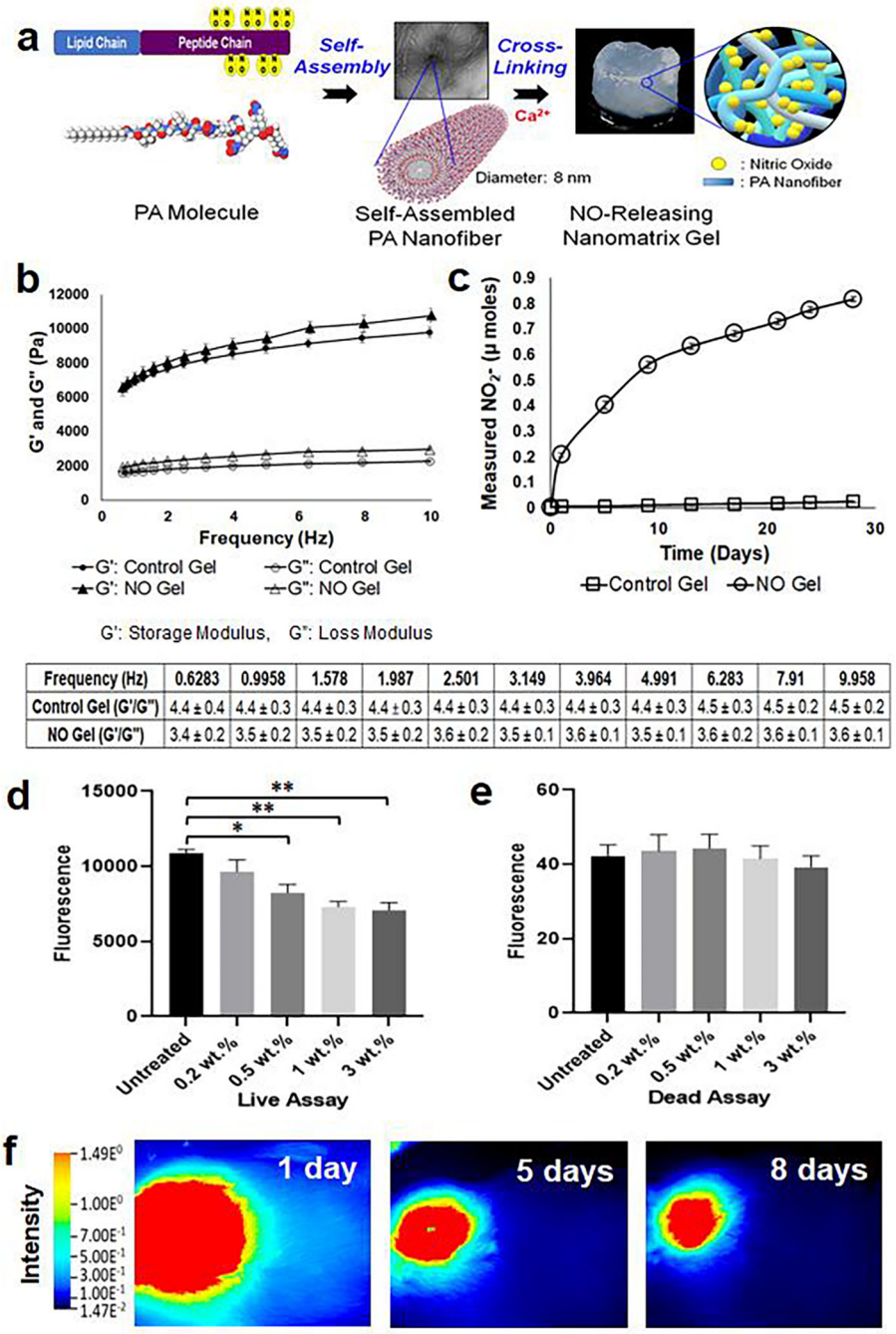

Frequency (Hz)	0.6283	0.9958	1.578	1.987	2.501	3.149	3.964	4.991	6.283	7.91	9.958
Control Gel (G'/G")	4.4 ± 0.4	4.4 ± 0.3	4.4 ± 0.3	4.4 ± 0.3	4.4 ± 0.3	4.4 ± 0.3	4.4 ± 0.3	4.4 ± 0.3	4.5 ± 0.3	4.5 ± 0.2	4.5 ± 0.2
NO Gel (G'/G")	3.4 ± 0.2	3.5 ± 0.2	3.5 ± 0.2	3.5 ± 0.2	3.6 ± 0.2	3.5 ± 0.1	3.6 ± 0.1	3.5 ± 0.1	3.6 ± 0.2	3.6 ± 0.1	3.6 ± 0.1

Fig. 3. Characterization of NO gel.

(**a**) Formation of NO releasing nanomatrix gel by self-assembly and cross-linking of PA molecules. (**b**) Measure of storage modulus (G') and loss modulus (G") of nanomatrix gels over various frequencies (0–10 Hz) using dynamic oscillatory rheometry at 37°C. G'/G" of nanomatrix gels is calculated in the table. Data are presented as the mean ± s.e.m. (n=4 of each group). (**c**) Evaluation of *in vitro* NO release profiles from nanomatrix gels for 28 days. NO released samples from each time point were analyzed using the total NO assay kit, which measured the nitrite (NO_2-; primary degradation product of NO) and the reduced

NO_2- from nitrate (NO_3-). Data are presented as the mean ± s.e.m. NO releasing nanomatrix gel (n=4) and control nanomatrix gel without NO (n=3). (**d**) Live and (**e**) dead assays on SMCs after 3-day culture with varied concentrations of PA-YK-NO (0.2, 0.5, 1, and 3 wt.%) containing nanomatrix gels. Data is presented as the mean ± s.e.m. (n=4 for each group). *p<0.05 and **p<0.01. An unpaired t-test was used to test for statistical differences between groups. (**f**) Degradation of NO releasing nanomatrix gel at the rat femoral AVF. The IR fluorescence dye was conjugated to the PA for *in vivo* visualization of gel using LiCOR Pearl Trilogy machine at various time points (up to 57 days; see Supplementary Fig. S3; representative images from one rat (n=3)).

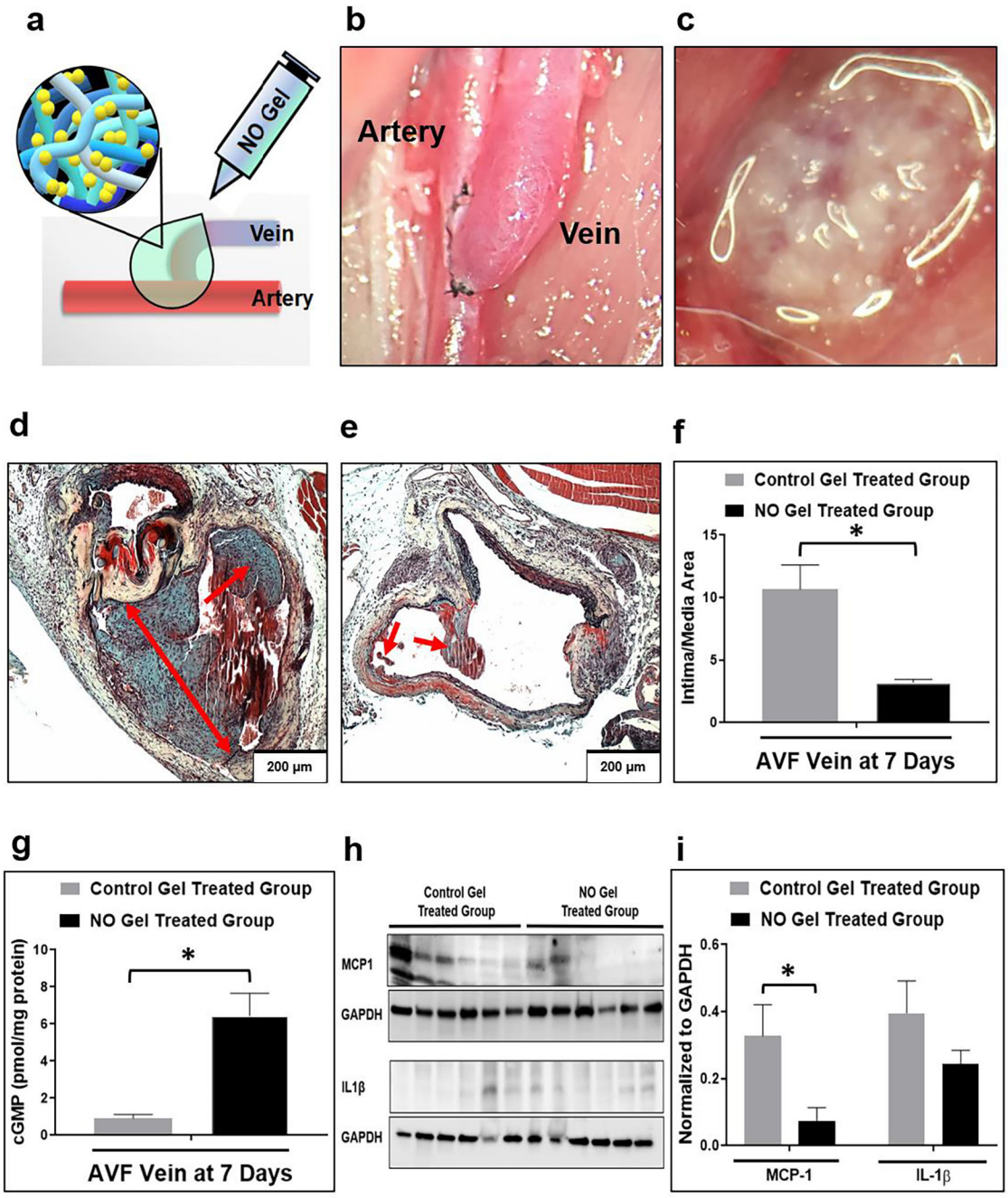

Fig. 4. Effects of NO gel treatment, 7 days following AVF creation in rats.

(**a**), (**c**) Application of NO releasing nanomatrix gel immediately after AVF creation. (**b**) Rat femoral (end) vein to artery (side) AVF model. (**d**) Representative histological images of venous intimal hyperplasia development following 7-day post-AVF creation with the control gel treated group (note the level of aggressive intimal hyperplasia) and (**e**) the NO releasing nanomatrix gel treated group (note the limited intimal hyperplasia formation). Arrows: Intimal hyperplasia development. (**f**) Morphometric analysis from AVF veins. Data are presented as the mean ± s.e.m. (n=4 for each group). *p<0.05. (**g**) cGMP concentration in AVF veins measured using ELISA. Data are presented as the mean ± s.e.m. (n=4 for

control gel treated group and n=3 for NO gel treated group). *p<0.05. (**h**), (**i**) Representative Western blots and densitometric analysis of MCP-1 and IL-1β protein expression from AVF-veins. Equivalence of loading was assessed by immunoblotting for GAPDH. Data are presented as the mean ± s.e.m. (n=6 for each group). *p<0.05. An unpaired t-test was used to test for statistical differences between control gel treated and NO gel treated groups.

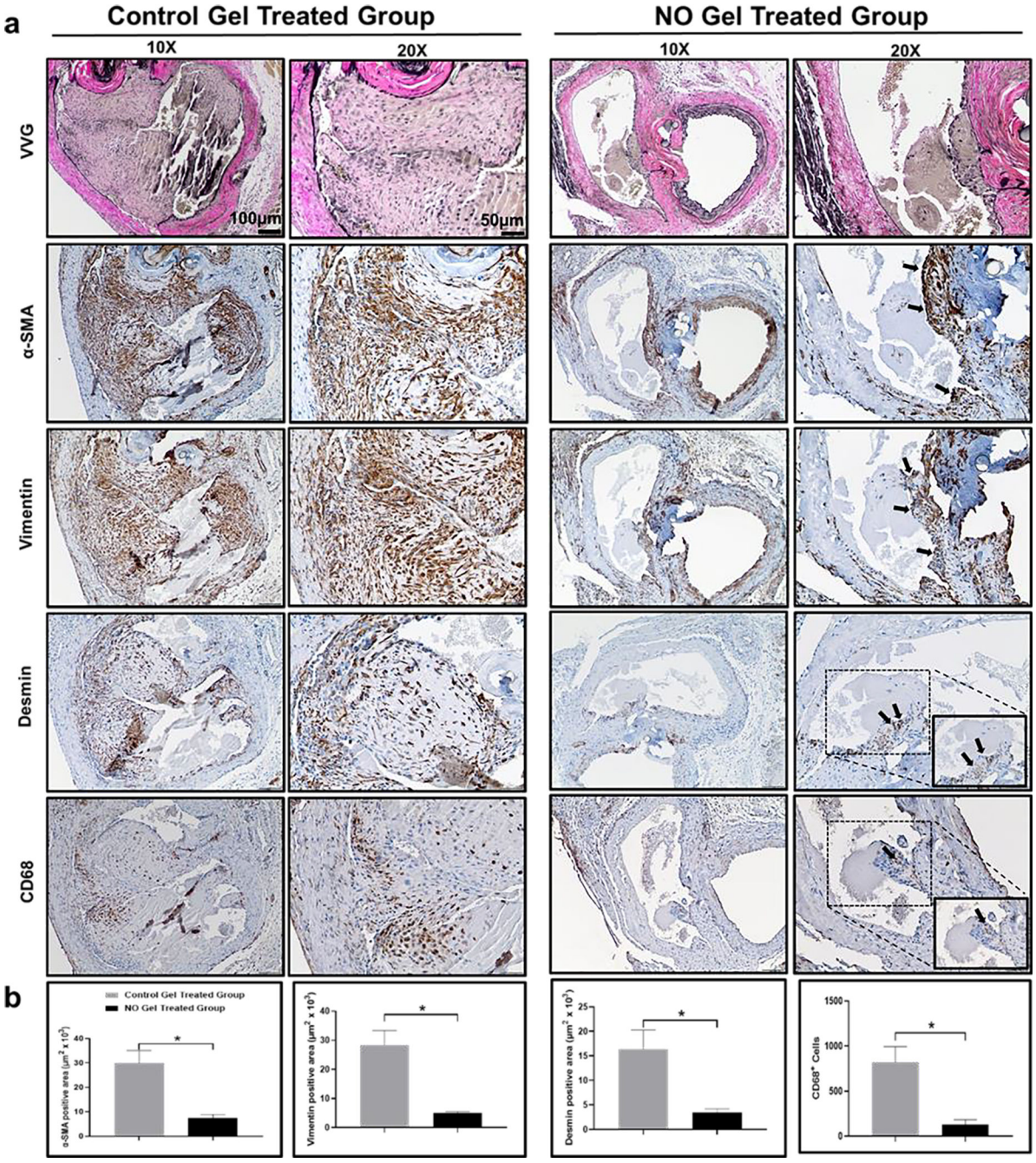

Fig. 5. Expression of α-SMA, Vimentin, Desmin and CD68 following NO gel treatment in rat AVF veins.

(a) Immunostaining of representative sections from control gel and the NO-releasing nanomatrix gel treated groups. Higher magnification boxed images are at 40x. (b) Quantification of α-SMA, Vimentin, Desmin positive area and CD68 cells in the intimal region. Black arrows: positive regions. N = 3 in each group. *$p < 0.05$.

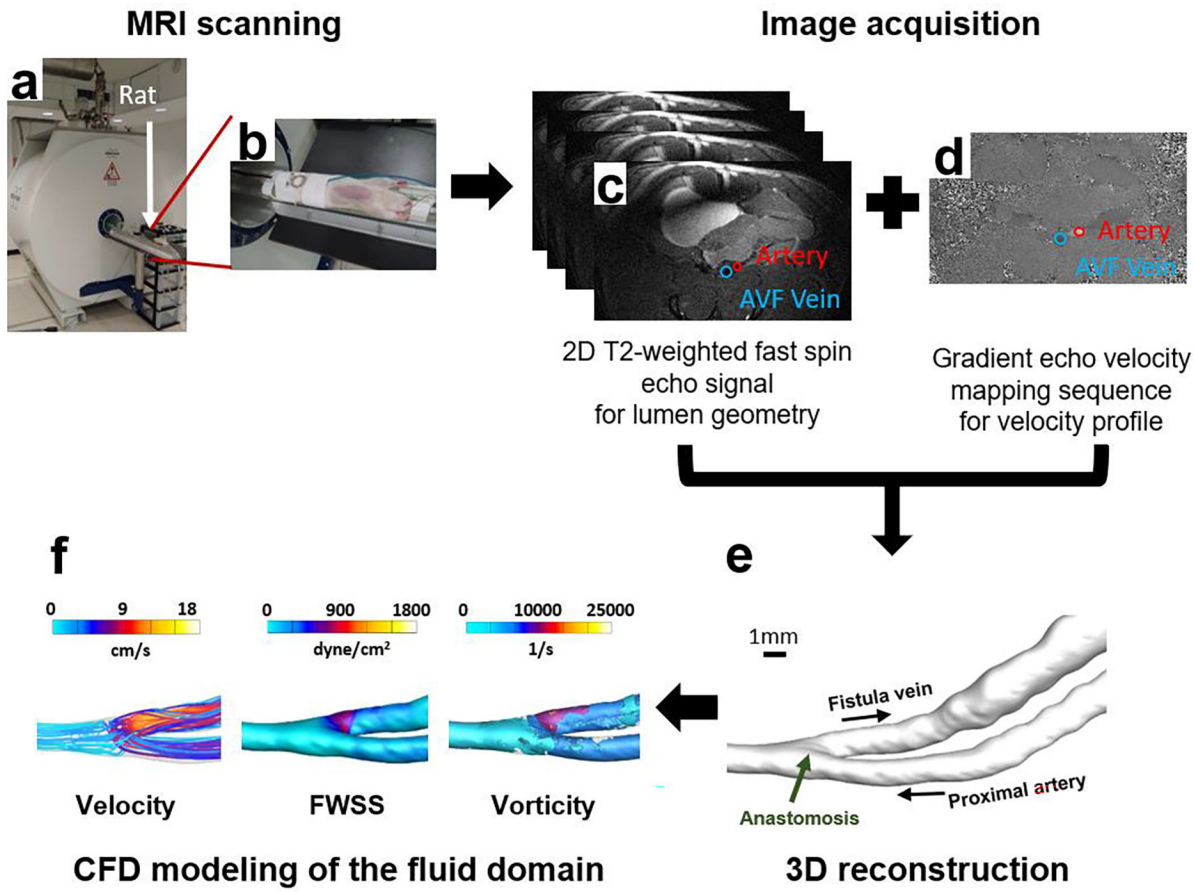

Fig. 6. MRI analysis of rat AVF.

(**a**), (**b**) MRI scanning of a rat using a Bruker Biospec 9.4T/20-cm horizontal bore instrument. (**c**) Image acquisition with a T2-weighted fast spin sequence (black-blood double inversion) for visualization of AVF lumen geometry. (**d**) Gradient echo velocity mapping sequence for quantitative measures of the blood flow. (**e**) 3D smoothed geometric reconstruction of the AVF lumen. (**f**) MRI data extraction and CFD simulation of the fluid domain.

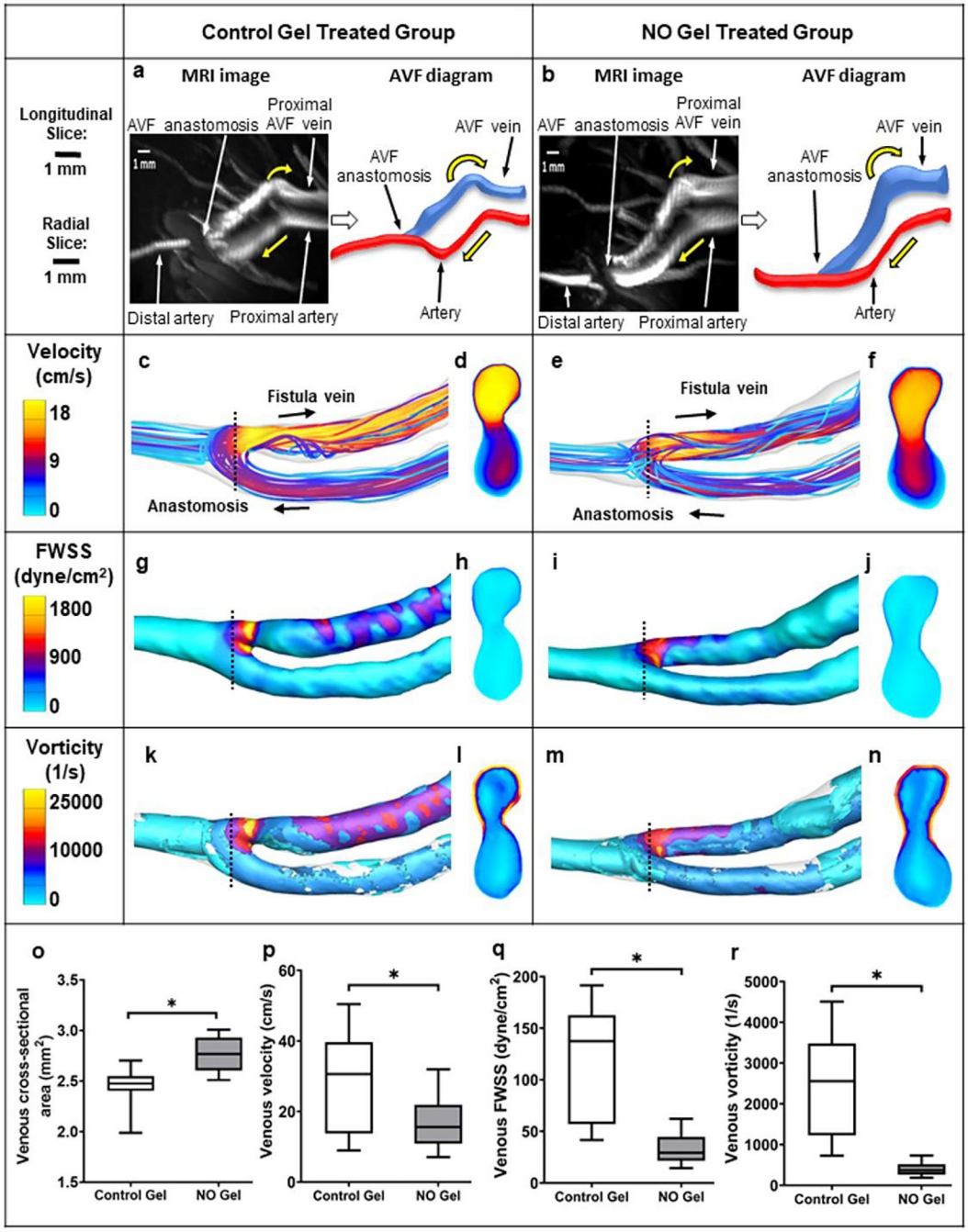

Fig. 7. Hemodynamics at the rat AVF at 7 days after NO gel treatment.

(**a**), (**b**) MRI images of rat AVFs treated with the control gel without NO and the NO releasing nanomatrix gel, respectively. Yellow arrow: blood flow direction. (**c-n**) Color maps of the velocity, FWSS, and vorticity, as well as the cross-section (located at the dashed black lines) of rat AVFs. Black arrow: blood flow direction. (**o**) venous cross-sectional area. (**p-r**) CFD quantifications of venous velocity, venous FWSS, and venous vorticity, respectively. Box and whisker plots present data from the 25th to 75th percentile with whiskers extending

to the 5th and 95th percentile. (n=3 for the control gel treated group and n=4 for the NO gel treated group). *$p<0.05$.

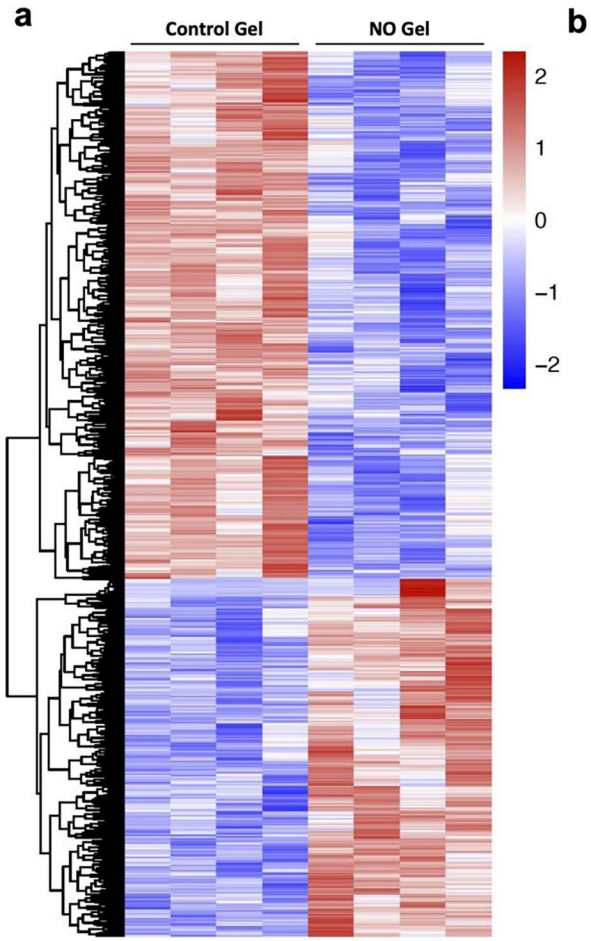

b

Pathway	Z score (-3 Reduced 0 Increased 3)	p-value
IL-15 Production		7.94E-05
Regulation Of The Epithelial Mesenchymal Transition		1.70E-05
Cardiac Hypertrophy Signaling (Enhanced)		2.00E-11
HOTAIR Regulatory Pathway		3.31E-06
WNT/Ca+ pathway		2.09E-04
G Beta Gamma Signaling		3.55E-03
Cardiac Hypertrophy Signaling		2.51E-09
FGF Signaling		6.46E-04
HIF1α Signaling		6.31E-05
cAMP-mediated signaling		3.47E-03
Estrogen Receptor Signaling		3.16E-12
Senescence Pathway		1.70E-05
Gαq Signaling		3.39E-03
Insulin Receptor Signaling		1.29E-04
STAT3 Pathway		2.51E-04
Dilated Cardiomyopathy Signaling Pathway		1.17E-07
ERK5 Signaling		7.24E-03
Cardiac β-adrenergic Signaling		1.78E-03
IL-8 Signaling		2.88E-03
IL-7 Signaling Pathway		1.17E-03
IGF-1 Signaling		1.38E-03
IL-3 Signaling		4.37E-03
Endothelin-1 Signaling		4.68E-07
PDGF Signaling		7.94E-04
P2Y Purigenic Receptor Signaling Pathway		4.37E-05
Signaling by Rho Family GTPases		3.80E-05
Thrombopoietin Signaling		2.95E-03
BMP signaling pathway		8.71E-03
ERK/MAPK Signaling		6.46E-04
Apelin Endothelial Signaling Pathway		1.17E-04
VEGF Signaling		7.24E-05
Relaxin Signaling		1.07E-03
VEGF Family Ligand-Receptor Interactions		2.19E-03
Inhibition of Matrix Metalloproteases		1.10E-05
Notch Signaling		3.63E-04
Gαi Signaling		6.46E-03
Renin-Angiotensin Signaling		6.17E-04
Ephrin Receptor Signaling		6.76E-04
Paxillin Signaling		1.95E-03
RAC Signaling		6.46E-03
IL-2 Signaling		8.32E-03
Regulation of Actin-based Motility by Rho		9.77E-03
PPARα/RXRα Activation		6.17E-06
PI3K/AKT Signaling		1.45E-03
Gα12/13 Signaling		4.68E-03

C

Upstream Regulator	Type	Z score (-4 Inactivated 0 Activated 4)	p-value
TGFB1	growth factor		8.48E-12
CCR2	g-protein coupled receptor		4.17E-06
IL1B	cytokine		2.98E-03
IL6	cytokine		1.14E-03
IGF1	growth factor		3.33E-11
TGFB3	growth factor		2.70E-06
cyclic AMP	chemical - endogenous mammalian		1.30E-04
BMP4	growth factor		1.53E-03
IL13	cytokine		2.39E-03
BMP10	growth factor		7.82E-05
TNF	cytokine		5.21E-09
BMP2	growth factor		2.67E-04
NOTCH4	transcription regulator		4.14E-05
VEGFA	growth factor		2.08E-03
TGFBR1	kinase		6.06E-05
PDGFB	growth factor		1.57E-06
BMP7	growth factor		5.10E-06
NOTCH1	transcription regulator		1.03E-06
PDGFC	growth factor		1.10E-05
EPHB4	kinase		6.42E-03
KLF4	transcription regulator		6.83E-05
IL2	cytokine		9.01E-03
RUNX2	transcription regulator		5.83E-06
FGF1	growth factor		3.28E-05
ADAM12	peptidase		1.12E-06
MMP2	peptidase		9.96E-04
NOS3	enzyme		8.51E-04
mir-455	microrna		3.62E-05
ADAMTS12	peptidase		1.65E-03
SMAD7	transcription regulator		1.97E-08

Figure 8. Transcriptomics of NO-gel versus control gel.

(A) Hierarchical clustering of the log2 normalized counts from 1267 significant genes. The values are scaled by rows and represent the number of standard deviations from the mean log2 normalized count. (B) Canonical pathways with activation z-scores and p-values from Ingenuity Pathway Analysis. (C) Upstream regulators with activation z-scores and p-values from Ingenuity Pathway Analysis. The activation Z-score makes predictions about the direction of gene regulation (inhibited or activated).